VIP

Organic Spin Clusters: Annelated Macrocyclic Polyarylmethyl Polyradicals and a Polymer with Very High Spin $S = 6$–18

Andrzej Rajca,*[a] Jirawat Wongsriratanakul,[a] Suchada Rajca,[a] and Ronald L. Cerny[b]

Abstract: Synthesis and magnetic studies of annelated macrocyclic polyradicals and a related high-spin polymer with macrocyclic repeat units are described. Polyarylmethyl polyether precursors to the polyradicals and the related polymer are prepared by using Negishi cross-coupling of difunctionalized calix[4]arene-based macrocycles. The three lowest homologues, with high degree of monodispersity, are tetradecaether (14-ether) **3-$(OCH_3)_{14}$**, octacosaether (28-ether) **4-$(OCH_3)_{28}$**, and dotetracontaether (42-ether) **5-$(OCH_3)_{42}$**, in which 2, 4, and 6 calix[4]arene-based macrocycles are annelated to the center macrocycle, respectively. The evidence for their annelated structures (ladder connectivities) is based upon FAB-MS and the ^{1}H NMR based end-group analysis. The absolute masses (4–12 kDa) were determined by FAB-MS and GPC/MALS. Small angle neutron scattering (SANS) provides the radii of gyration of 1.7, 2.0, and 3.2 nm for **4-$(OCH_3)_{28}$**, **5-$(OCH_3)_{42}$**, and polymer **6-$(OCH_3)_n$**, respectively. The corresponding polyarylmethyl polyradicals **3** and **4**, and polymer **6** possess average values of $S \approx 6$–7, $S \approx 10$, and $S \approx 18$, respectively, as determined by SQUID magnetometry and numerical fits to linear combinations of Brillouin functions. The quantitative values of magnetization at saturation and of magnetic susceptibilities indicate that about 40–60% of unpaired electrons are present at low temperatures ($T =$ 1.8–5 K). For polyradical **3**, the variable temperature magnetic data are fit to the Heisenberg Hamiltonian based model. The variable magnetic field data at low temperatures are also fit to a percolation-based model for organic spin cluster, with random distribution of chemical defects, and ferromagnetic versus antiferromagnetic couplings, providing quantitative agreement between the experiment and the theory. For polyradical **3** (with $S \approx 6$–7), annealing at room temperature for 0.5 h leads to a polyradical with $S \approx 5$.

Keywords: high-spin systems · macrocycles · magnetic properties · polymers · radicals

Introduction

Organic molecules and polymers with very high values of spin quantum number S are important for the design of organic magnetic materials based upon through-bond magnetic interactions (exchange coupling).[1–12] For such organic polymer magnets to possess long-range magnetic ordering at relatively high temperatures, effective dimensionality above two for pairwise exchange coupling between the electron spins ("unpaired electrons") is required.[13–16] Recent discovery of magnetic ordering in conjugated organic polymer **1**, at temperature of about 10 K, provides an impetus for investigation of its effective dimensionality of the π-conjugated network as one of the contributing factors to the magnetic ordering.[17–19]

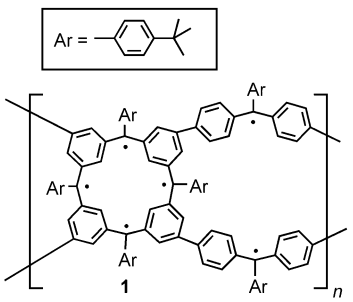

1

[a] Prof. A. Rajca, J. Wongsriratanakul, Dr. S. Rajca
Department of Chemistry, University of Nebraska
Lincoln, NE 68588-0304 (USA)
Fax: (+1) 402-472-9402
E-mail: arajca1@unl.edu

[b] Dr. R. L. Cerny
Department of Chemistry
and Nebraska Center for Mass Spectrometry
University of Nebraska, Lincoln, NE 68588-0304 (USA).

Supporting information for this article is available on the WWW under http://www.chemeurj.org/ or from the author. Experimental section [materials and special procedures, NMR spectroscopy and other analyses, small angle neutron scattering, synthetic details for model compounds **13-$(OCH_3)_6$BrH**, **14-$(OCH_3)_6H_2$**, and **11-$(OCH_3)_{27}H_2$**]; ^{1}H NMR spectra [for **3-$(OCH_3)_{14}$**, **4-$(OCH_3)_{28}$**, **5-$(OCH_3)_{42}$**, **12-$(OCH_3)_n$**, and polymer **6-$(OCH_3)_n$**]; FAB-MS high-resolution scans for selected polyethers; summary plot and summary table of GPC/MALS data; summary of low-resolution FAB-MS [for **3-$(OCH_3)_{14}$**, **4-$(OCH_3)_{28}$**, **5-$(OCH_3)_{42}$**, **12-$(OCH_3)_n$**, and polymer **6-$(OCH_3)_n$**]; details of magnetic measurements and data fitting.

DOI: 10.1002/chem.200306036

In the synthesis of polymer **1**, the final C–C bond connectivity is controlled in the polymerization step, in which two macrocyclic tetrafunctionalized monomers are condensed by means of Negishi cross-coupling.[17,20] One of the two limiting modes of cross-linking during such polymerization, leading to the annelated macrocyclic structures, is shown in Figure 1.[21] The larger-sized cross-linking macrocycles would

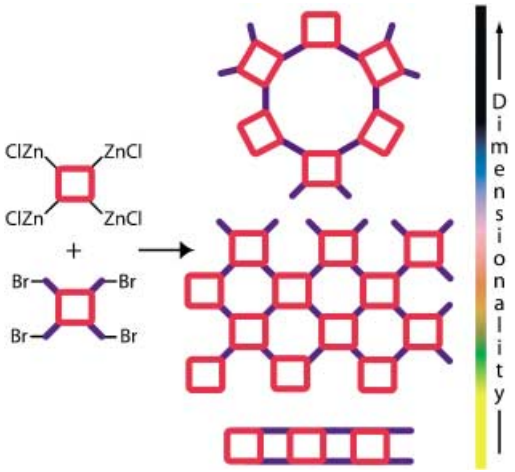

Figure 1. One of the possible annelation modes in polymer **1**.

correspond to higher dimensionality of the formed network. It would be important to determine whether formation of such annelated macrocycles is feasible, especially for better understanding of structure of polymer **1**, in relation to the observed magnetic ordering.

To date, synthesis of annelated macrocyclic polyradicals has been limited to the $S \approx 6$ polyradical **2**.[22] In polyradical **2**, annelation leads to two problems: 1) weakening of the ex-

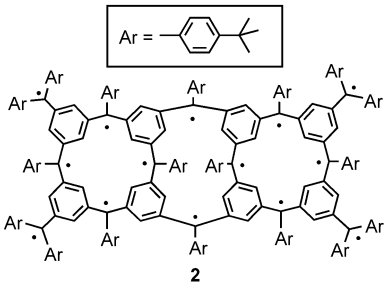

change coupling and 2) increased reactivity of radicals, through severe out-of-plane distortion of the π-system.[22]

Herein we report synthesis and magnetic characterization of novel annelated macrocyclic polyradicals **3** and **4**, and related polymer **6** with a macrocyclic repeat unit. Polyradicals **3** and **4**, and polymer **6** may be viewed as fragments of polymer **1**. (Polyradicals with the linear and branched connectivities of macrocycles, which are one-dimensional models for polymer **1**, are reported elsewhere.[19]) The synthesis of an-

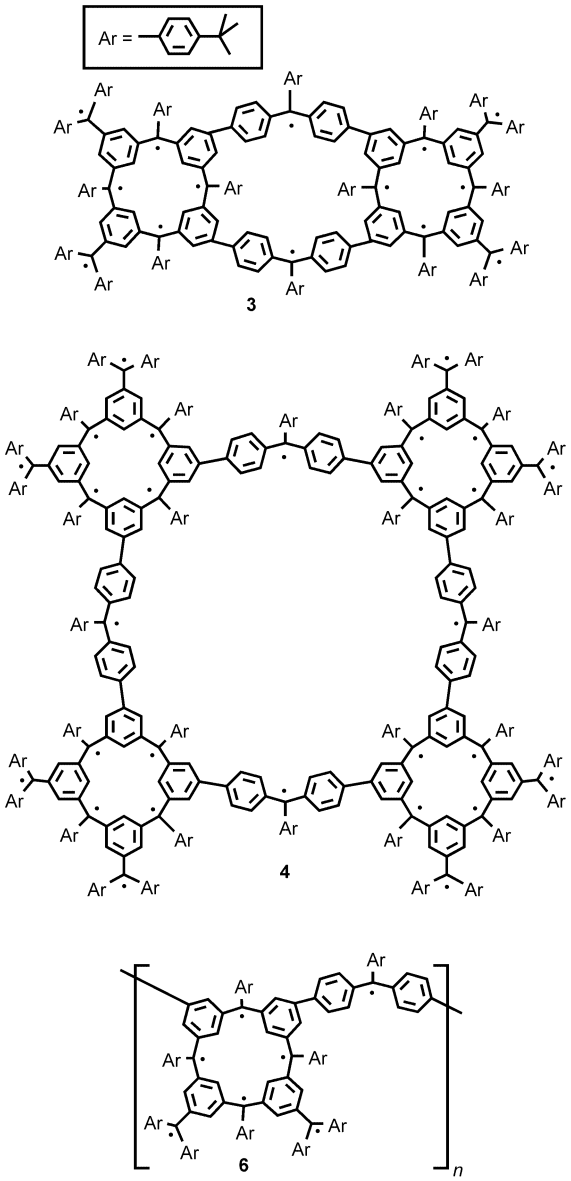

nelated macrocyclic polyethers corresponding to **3** and **4**, and their higher macrocyclic homologues indirectly addresses the critical question of dimensionality of polymer **1**. Compared with the previously reported annelated macrocyclic polyradical **2**, it is expected that the use of bis(biphenylene)-methyl (in **3**), instead of bis(phenylene)methyl (in **2**), as annelating linkages, should provide greater resonance stabilization of the triarylmethyl radicals, decreasing the density of chemical defects.[19] Indeed, magnetic studies show that polyradical **3** has somewhat higher values of S than polyradical **2**. The values of S increase along the homologous series, from $S \approx 6$–7 for **3** to $S \approx 18$ for polymer **6**. With the exception of polymer **1**, the value of $S \approx 18$ for polymer **6** exceeds by far the best results ($S \approx 5$) in the previously reported organic high-spin polymers.[7–11,24]

Results and Discussion

Synthesis: Annelated macrocyclic polyethers **3-$(OCH_3)_{14}$**, **4-$(OCH_3)_{28}$**, **5-$(OCH_3)_{42}$**, and polymer **6-$(OCH_3)_n$**, were obtained by condensation of difunctionalized macrocyclic monomers **7-$(OCH_3)_6Br_2$** and **8-$(OCH_3)_8Br_2$** (Scheme 1). The intermediate chromatographic fraction (between **5-$(OCH_3)_{42}$** and **6-$(OCH_3)_n$**), that is, polyether **12-$(OCH_3)_n$**, was isolated as well. In addition, a "linear" reference compound for annelated macrocyclic polyether **4-$(OCH_3)_{28}$**, that is, polyether **11-$(OCH_3)_{27}H_2$**, was prepared (Scheme 1).

Negishi coupling of the organozinc derivative of monomer **7-$(OCH_3)_6Br_2$** with linker **9** (3 equiv) gave monomer **8-$(OCH_3)_8Br_2$** in 45–56% yield. Small amounts of side product **10-$(OCH_3)_{15}Br_2$** (3–4%) were also isolated. The two monomers (each ~0.01 M) were polymerized by using Negishi coupling; the organozinc derivative of monomer **7-$(OCH_3)_6Br_2$** was treated with monomer **8-$(OCH_3)_8Br_2$** to give a mixture of the annelated macrocyclic and polymeric polyethers in ~60% overall isolated yields. Notably, the yields for all three annelated macrocycles are similar, that is, approximately several percent with decreasing level of purity for the higher homologues.

For each condensation, numerous chromatographic fractions were obtained and analyzed with FAB-MS (Tables 1s–3s in the Supporting Information). As found for other homologous polyarylmethyl polyethers, lower R_f values on normal-phase silica gel correlate with higher molecular masses. For the tetradecaether (14-ether) **3-$(OCH_3)_{14}$**, the relative peak height amplitude in FAB-MS is 100% versus 2% for the side products. For the octacosaether (28-ether) **4-$(OCH_3)_{28}$** and its higher homologue dotetracontaether (42-ether) **5-$(OCH_3)_{42}$**, FAB-MS data show increasing relative peak heights corresponding to side products, including linearly connected calix[4]arenes. The isolated yields (after chromatography) reported in Scheme 1 should be viewed as approximate.

Polyethers **11-$(OCH_3)_{27}H_2$** and **14-$(OCH_3)_6H_2$** were prepared to provide model compounds for the end-group analysis of the annelated macrocycles. Calix[4]arene **7-$(OCH_3)_6Br_2$** was subjected to Li/Br exchange, followed by MeOH quenching, to give calix[4]arenes **13-$(OCH_3)_6BrH$** and **14-$(OCH_3)_6H_2$**. Because the starting calix[4]arene **7-$(OCH_3)_6Br_2$** has no elements of symmetry,[20] **13-$(OCH_3)_6BrH$** was isolated as mixtures of two isomers. Negishi coupling of the organozinc derivative of **13-$(OCH_3)_6BrH$** (from a fraction containing two isomers, 1:0.8) with **10-$(OCH_3)_{15}Br_2$** (0.4 equiv) gave cross-coupling products **11-$(OCH_3)_{27}H_2$** and **15-$(OCH_3)_{21}BrH$** in 7% yields (Scheme 1).[25]

Characterization of polyethers: All polyethers obtained in this work, including those isolated as a single diastereomers, have glassy-like, poorly defined melting behavior. The IR

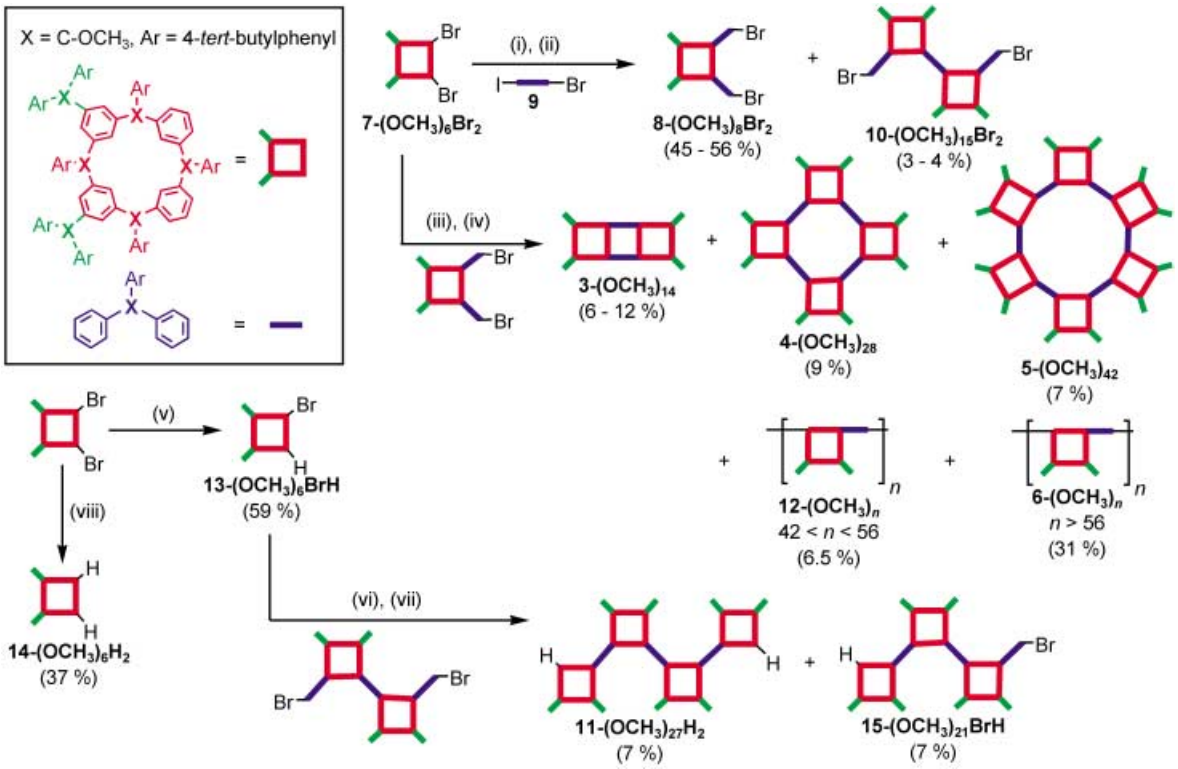

Scheme 1. Synthesis of polyethers: i) *t*BuLi, THF, −78°C for 2 h, then −20°C for 10 min, then $ZnCl_2$, −78°C to room temperature for 3 h; ii) $[Pd(PPh_3)_4]$ (3 mol% per CC bond), 100°C, 1.5 d; iii) *t*BuLi, THF, −78°C for 2.5 h, then −20°C for 15 min, then $ZnCl_2$, −78°C to room temperature for 2.5 h; iv) $[Pd(PPh_3)_4]$ (3.7 mol% per CC bond), 100°C, 2 d; v) *n*BuLi, diethyl ether, −78°C for 1 h, then −20°C for 10 min, then MeOH, −78°C to room temperature; vi) *t*BuLi, THF, −78°C for 3 h, then −20°C for 10 min, then $ZnCl_2$, −78°C to room temperature for 4 h; vii) $[Pd(PPh_3)_4]$ (4.2 mol% per CC bond), 100°C, 2 d; viii) *t*BuLi, diethyl ether, −78°C for 2.5 h, then −20°C for 10 min, then MeOH, −78°C to room temperature.

spectra possess a strong band at about 1080 cm^{-1}, characteristic of the C–O–C triarylmethyl methyl ether group.

Monomer **7-$(OCH_3)_6Br_2$** corresponds to the previously reported C_1-symmetric *cis*/*trans* isomer (with the highest R_f value on silica).[22] Because monomer **7-$(OCH_3)_6Br_2$** and linker **9** are used as racemic mixtures, four and sixteen diastereomers are possible for monomer **8-$(OCH_3)_8Br_2$** and side product **10-$(OCH_3)_{15}Br_2$**, respectively.

FAB-MS for monomer **8-$(OCH_3)_8Br_2$** and side product **10-$(OCH_3)_{15}Br_2$** give the expected $[M-OCH_3]^+$ ion clusters centered at $m/z \approx 2409$ and 4362, respectively. The corresponding high-resolution spectra reveal the $[M-OCH_3]^+$ ion clusters with the isotopic spacing of $m/z \approx 1$ and the isotopic intensities that match those calculated for the respective formulas $C_{163}H_{179}O_7Br_2$ and $C_{303}H_{337}O_{14}Br_2$.

The ^{1}H NMR spectra for **8-$(OCH_3)_8Br_2$** and **10-$(OCH_3)_{15}Br_2$** in [D_6]benzene at 293, 328, and 348 K are rather complicated. For **8-$(OCH_3)_8Br_2$**, four types of the 1,3,5-trisubstituted benzene rings (rings A, B, C, D) are fairly well resolved in the aromatic region of the ^{1}H NMR spectrum at 348 K. Two of these 12 one-proton resonances either appear as two $J=2$ triplets ($\Delta\delta \approx 0.001$–$0.002$ ppm) or are broadened. These additional splittings are less noticeable in the more spectrally overlapped 1,4-disubstituted benzene-ring region. In this region, 24 two-proton doublets ($J=$ 8–9 Hz), which are correlated pairwise in the COSY spectrum, account for twelve 1,4-disubstituted benzene rings. However, the thirteenth and fourteenth ring appear as overlapped AB systems. Spectral patterns in the 2.9–3.1 ppm chemical shift region at 293, 328, and 348 K are consistent with eight methoxy groups; however, one of the three-proton resonances is further split ($\Delta\delta \approx 0.002$ ppm) into two singlets and the other three-proton resonance is broadened at 293 K. In the *tert*-butyl group region, eight nine-proton singlets and one 18-proton resonance are found at 293, 328, and 348 K; at 293 K, the 18-proton resonance splits into two singlets. The number of resolved resonances in ^{13}C NMR spectra (obtained at 293 K only) is less than expected for a single diastereomer; only one resonance (at 121.6 ppm) is detected for C–Br group. These analyses are consistent with the structure of **8-$(OCH_3)_8Br_2$**, isolated as mixture of diastereomers, which possess nearly identical, overlapping chemical shifts.

A relatively large number of possible diastereomers and a more complex structure for side product **10-$(OCH_3)_{15}Br_2$** is reflected by the more spectrally congested ^{1}H NMR spectra ([D_6]benzene, 293, 328, and 348 K), relative to those for **8-$(OCH_3)_8Br_2$**. ^{13}C NMR spectra possess inadequate signal-to-noise ratios and resolution for meaningful analysis and, therefore, are not reported. In the best-resolved ^{1}H NMR spectrum at 348 K, eight types of the 1,3,5-trisubstituted benzene rings can be identified. However, for two of those rings, not all the expected six cross-peaks are observed: in one of those two rings, only two cross-peaks are found and in the other ring, two resonances are nearly degenerate ($\Delta\delta \approx 0.01$ ppm); thus only four cross-peaks are found at the spectral resolution of the COSY experiment. The resonances from the expected 25 unique 1,4-disubstituted benzene rings (for one diastereomer) are too complex for analysis with simple COSY experiments. In the methoxy group region of the ^{1}H NMR spectra, 15 distinct three-proton singlets are expected for each diastereomer. However, 22 resonances, with noninteger integrations and complex spectral pattern, are observed. Similarly, the spectral pattern in the *tert*-butyl region is more complex than expected for a single diastereomer.

For the target annelated macrocyclic polyethers, both large number of diastereomers and conformational restriction of annelation are expected to lead to complicated ^{1}H NMR spectra (Figures 1s and 2s in the Supporting Information). Distinct spectral patterns in the methoxy and aromatic regions are found for the lowest homologue, **3-$(OCH_3)_{14}$**. Its methoxy group and aromatic regions consist of relatively large number of resonances with the relatively wide chemical shift range, relative to the spectra for the higher homologues (Figures 1s and 2s in the Supporting Information).The ^{1}H NMR spectra for the higher homologues, including polymer **6-$(OCH_3)_n$**, are nearly indistinguishable from each other. At 293 K, the methoxy group region possesses three major broad resonances at 3.10, 2.97, 2.91 ppm (1:2:4); this is consistent with the relative numbers of the linker, calix[4]arene outer, and calix[4]arene inner triarylmethyl positions in the heptaether repeat unit (Scheme 1). However, these tentative assignments should be viewed with caution, because the ^{1}H NMR spectra at 331 and 348 K reveal increasingly complex patterns for the methoxy region of **4-$(OCH_3)_{28}$** (Figure 3s in the Supporting Information).

^{1}H NMR spectra of aromatic regions for the polyethers **3-$(OCH_3)_{14}$**, **4-$(OCH_3)_{28}$**, **5-$(OCH_3)_{42}$**, **12-$(OCH_3)_n$**, and **6-$(OCH_3)_n$** provide evidence for the annelated macrocyclic (with no end groups) versus linear macrocyclic (with end groups) structures. The linear macrocyclic structures may be obtained, when one of the reactive ends (ZnCl or Br) in the polymerization intermediates is quenched with a proton or hydrogen atom (hydrogen end group). FAB-MS analyses (Tables 1s–3s in the Supporting Information) show minor peaks at m/z corresponding to such products. The linear macrocyclic structures with Br end groups are less significant, according to the FAB-MS analyses, though they are detectable in selected samples of **3-$(OCH_3)_{14}$** and **5-$(OCH_3)_{42}$**. Therefore, verification for the annelated macrocyclic structures is based upon the hydrogen end-group analysis.

The hydrogen end groups may be formed at either the calix[4]arene or the linker ends; in either case, a spin system of at least three protons with $J \approx 8$ coupling constants is formed. In principle, the three-spin systems could be selectively detected by the triple quantum filtered COSY. However, with the increasing degree of polymerization, end groups become more difficult to detect. Therefore, **4-$(OCH_3)_{28}$** was selected for detailed analysis, as shown in Figure 2. In the aromatic region of **4-$(OCH_3)_{28}$**, resonances near the ^{13}C satellite peak of [D_5]benzene are of relatively small integration, and the highest peak in this region appears as a doublet. This resonance shows a cross-peak in double quantum-filtered COSY, but no correlation in triple quantum-filtered COSY could be detected. However, in **11-$(OCH_3)_{27}H_2$** and **14-$(OCH_3)_6H_2$**, model compounds with hy-

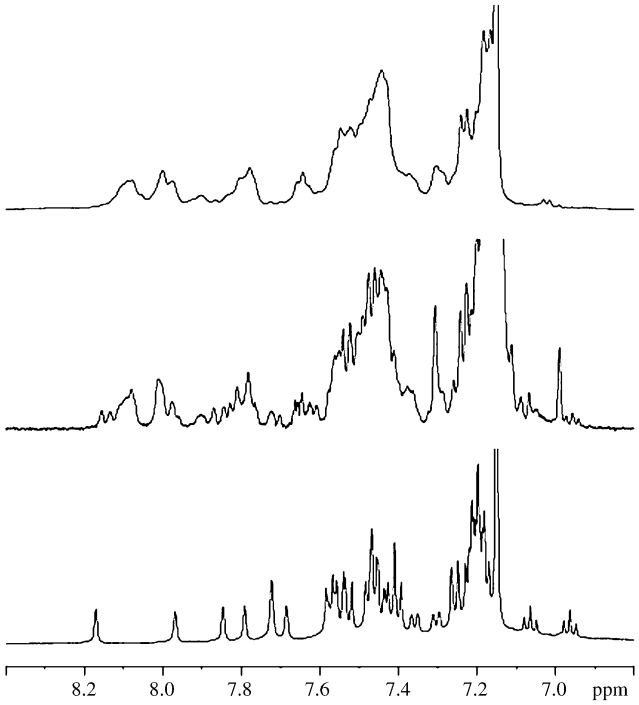

Figure 2. ^{1}H NMR (500 MHz, [D_6]benzene) spectra for **4-$(OCH_3)_{28}$** (top), **11-$(OCH_3)_{27}H_2$** (middle), and **14-$(OCH_3)_6H_2$** (bottom) at 293 K. The ^{13}C satellite [D_5]benzene peak appears at 6.990 ppm.

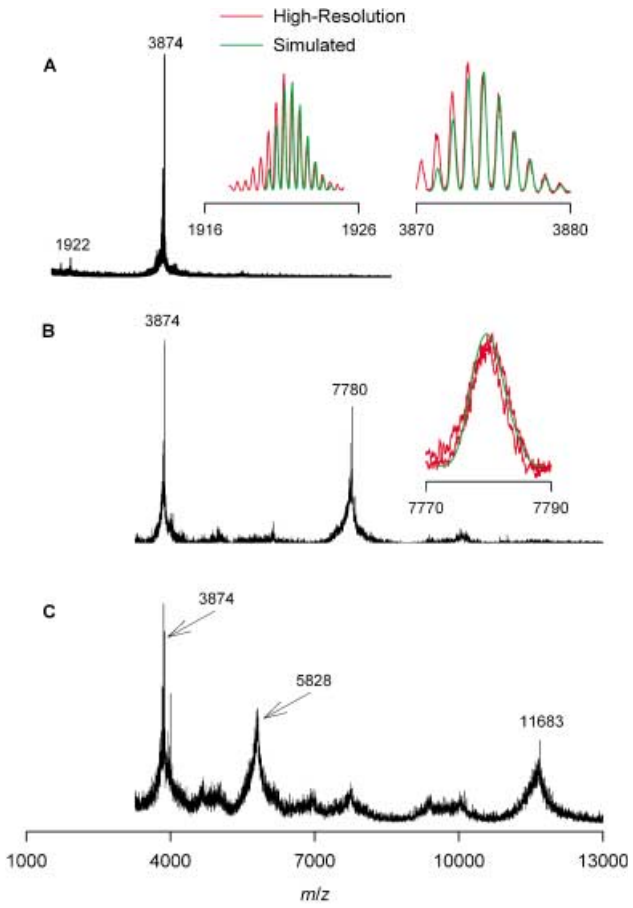

Figure 3. FAB-MS (ONPOE) for polyethers **3-$(OCH_3)_{14}$** (plot A), **4-$(OCH_3)_{28}$** (plot B), and **5-$(OCH_3)_{42}$** (plot C). Main plots: low-resolution spectra. Inset plots: high-resolution spectra (red lines) and simulations of the isotopic intensities at natural isotopic abundance (green lines) for the $[M-OCH_3]^+$ ion clusters (and $[M-2OCH_3]^{2+}$ ion cluster for **3-$(OCH_3)_{14}$**).

drogen end groups on the calix[4]arene ends, the end-group protons are found as $J \approx 8$ triplets, appearing on either side of the ^{13}C satellite peak of [D_5]benzene.

Because of insufficient sample amount, quantum-filtered COSY experiments on **11-$(OCH_3)_{27}H_2$** were not successful; for example, the relatively low intensity for the end group peaks versus the ^{13}C satellite peak (Figure 2). For **14-$(OCH_3)_6H_2$**, well-defined cross-peaks to the two $J \approx 8$ triplets in both double and triple quantum-filtered COSY experiments are obtained. Inspection of the aromatic regions for the ^{1}H NMR spectra of polyethers **5-$(OCH_3)_{42}$**, **12-$(OCH_3)_n$**, and **6-$(OCH_3)_n$** does not show clear $J \approx 8$ triplet resonances near the upfield ^{13}C satellite [D_5]benzene peak (Figure 1s in the Supporting Information). This circumstantial evidence supports the annelated macrocyclic structure for **4-$(OCH_3)_{28}$** and, probably, for its higher homologue.

FAB-MS provides the best evidence for the annelated macrocycle **3-$(OCH_3)_{14}$** and its higher homologues. The low-resolution FAB-MS of **3-$(OCH_3)_{14}$** shows dominant the cluster ion at $m/z \approx 3874$ and the less intense (ca. 10% relative amplitude) cluster ion at $m/z \approx 1922$. The high-resolution spectra reveal that the spacings between the isotopomers are $m/z \approx 1$ and 0.5 for the peaks at $m/z \approx 3874$ and 1922, respectively, as expected for the singly and doubly charged ions; simulation of their relative isotopic intensities at the natural abundance provides good agreement with the formulas $C_{279}H_{313}O_{13}$ and $C_{278}H_{310}O_{12}$ for the $[M-OCH_3]^+$ and $[M-2OCH_3]^{2+}$ ion clusters, respectively (Figure 3A). The cluster ion at $m/z \approx 5500$, which possesses very low intensity (<2% relative amplitude), corresponds to a singly charged ion cluster with isotopic spacing of $m/z \approx 1$. Simulation of the isotopic intensities is consistent with the formula $C_{395}H_{449}O_{19}$, that is, $[M-OCH_3]^+$ ion cluster for **16-$(OCH_3)_{20}H_2$**, a structure consisting of three linearly connected calix[4]arenes with the hydrogen end groups. Compound **16-$(OCH_3)_{20}H_2$** may be formed as a cross-coupling product from two monomers of **7-$(OCH_3)_6Br_2$** and one monomer of **8-$(OCH_3)_8Br_2$**, followed by protic quench of the two organozinc end groups. For the four best chromatographic samples of **3-$(OCH_3)_{14}$**, the relative amplitudes of the $[M-OCH_3]^+$ ion clusters for **16-$(OCH_3)_{20}H_2$** are in the 1–5% range (Table 1s in the Supporting Information.)

The low-resolution FAB-MS of **4-$(OCH_3)_{28}$** and **5-$(OCH_3)_{42}$** show two and three prominent peaks, respectively (Figure 3B and C). For **4-$(OCH_3)_{28}$**, peaks at $m/z \approx 7780$ and ≈ 3874 have similar fragmentation patterns, including spacings between the fragmentation ions and the widths of their isotopic envelopes. For **5-$(OCH_3)_{42}$**, peaks at $m/z \approx 11\,683$, ≈ 5828, and ≈ 3874 have similar fragmentation patterns; however, the spacings between the fragmentation ions and the widths of their isotopic envelopes in the $m/z \approx 5828$ region are about half of those at $m/z \approx 11\,683$ and ≈ 3874. This suggests that the peak at $m/z \approx 5828$ corresponds to a doubly charged ion cluster and the remaining four peaks arise from

singly charged ion clusters. The peaks at $m/z \approx 7780$ and ≈ 11683 are assigned to the $[M-OCH_3]^+$ ion clusters for **4-$(OCH_3)_{28}$** and **5-$(OCH_3)_{42}$**, respectively. The peak $m/z \approx 5828$ may correspond to the $[M-2OCH_3]^{2+}$ ion cluster for **5-$(OCH_3)_{42}$**. For both **4-$(OCH_3)_{28}$** and **5-$(OCH_3)_{42}$**, high-resolution spectra for the $m/z \approx 3874$ peaks and simulations of the relative isotopic intensities at the natural abundance provide good agreement with the formula $C_{279}H_{313}O_{13}$, that is, indistinguishable from the $[M-OCH_3]$ ion cluster for **3-$(OCH_3)_{14}$** (Figure 4s in the Supporting Information). For **5-$(OCH_3)_{42}$**, the ion cluster at $m/z \approx 3859$ is relatively intense, exceeding the maximum relative amplitude of the ion cluster at $m/z \approx$ 3874. This suggests that the $m/z \approx 3874$ peaks in the FAB-MS of **4-$(OCH_3)_{28}$** and **5-$(OCH_3)_{42}$** may correspond to either fragment ions or admixtures of small amounts of diastereomers of **3-$(OCH_3)_{14}$** with similar R_f values. (In addition for **5-$(OCH_3)_{42}$**, the $m/z \approx 3859$ peak could correspond to a derivative of **3-$(OCH_3)_{14}$**, in which one of the methoxy groups is replaced with the hydroxyl group.[26])

The assignments of the $[M-OCH_3]^+$ ion clusters are verified by the high-resolution spectra. For **4-$(OCH_3)_{28}$**, measurements of $[M-OCH_3]^+$ ion cluster for three different chromatographic samples give m/z 7779.9, 7780.2, and 7779.7. These values are in good agreement with the calculated average mass (7780.075) and peak maximum mass (7779.71) for formula $C_{559}H_{629}O_{27}$ of the $[M-OCH_3]^+$ ion cluster (Figures 3 and 4). Corresponding m/z values for **5-$(OCH_3)_{42}$** are at the extreme edge of the instrumental range and resolution; m/z 11683.1 and 11683.3 are obtained for the $[M-OCH_3]^+$ ion cluster, using two different chromatographic samples. These values are *lower* by 2 amu than expected for formula $C_{839}H_{945}O_{41}$ of the $[M-OCH_3]^+$ ion cluster. (Average mass of 11685.765 and peak maximum mass of 11685.45 are calculated at natural isotopic abundance.) Notably, if the structure were not an annelated macrocycle, but a linear chain of calix[4]arenes with hydrogen end groups, the mass-to-charge ratio would be *higher* by 2 amu. Such a lower than expected value in the $m/z \approx 10000$ range under similar experimental conditions has another precedent in the polyarylmethyl polyether, for which structure could be adequately analyzed by NMR spectroscopy.[19] Analogous, but smaller, shifts to lower m/z values are also clearly observed for **3-$(OCH_3)_{14}$** (Figure 3A) and other polyarylmethyl polyethers in high-resolution spectra of $[M-OCH_3]^+$ ion clusters with resolved isotopomers.[18,19] Overall, the high-resolution scans support the annelated macrocyclic structure for both **4-$(OCH_3)_{28}$** and **5-$(OCH_3)_{42}$**.

Both low- and high-resolution FAB-MS for **4-$(OCH_3)_{28}$** and the model compound **11-$(OCH_3)_{27}H_2$** were carried out under the identical conditions (subsequent experiments) (Figure 4). In the low-resolution FAB-MS for **11-$(OCH_3)_{27}H_2$**, the most prominent peaks at $m/z \approx 7452$ and ≈ 3710 correspond to the singly charged $[M-OCH_3]^+$ and the doubly charged $[M-2OCH_3]^{2+}$ ion clusters, respectively. Most likely, the other peaks correspond to the side products.[27] In particular, the prominent peak at $m/z \approx 3710$ appears as doubly charged $[M-2OCH_3]^{2+}$ ion cluster, unlike the singly charged fragment ion for **4-$(OCH_3)_{28}$** in the corresponding m/z region. The high-resolution spectra give good agreement with the calculated m/z values for the $[M-OCH_3]^+$ cluster ions at the natural isotopic abundance for both compounds; also, the doubly charged $[M-2OCH_3]^{2+}$ ion cluster for **8-$(OCH_3)_{27}H_2$** is confirmed, in contrast to the singly charged fragment ion for **4-$(OCH_3)_{28}$** in the similar relative m/z region (Figure 4).

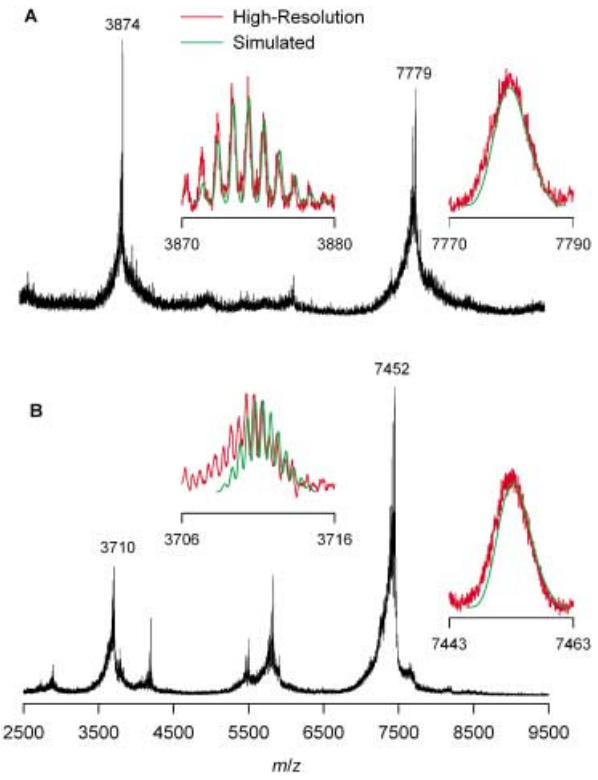

Figure 4. FAB-MS (ONPOE) for polyethers **4-$(OCH_3)_{28}$** (plot A) and **11-$(OCH_3)_{27}H_2$** (plot B) carried out under the identical conditions. Main plots: low-resolution spectra. Inset plots: high-resolution spectra (red lines) and simulations of the isotopic intensities at natural isotopic abundance (green lines) for the $[M-OCH_3]^+$ and $[M-2OCH_3]^{2+}$ ion clusters.

Gel-permeation chromatography with multiangle light-scattering (GPC/MALS) chromatograms of **3-$(OCH_3)_{14}$**, **4-$(OCH_3)_{28}$**, **5-$(OCH_3)_{42}$**, **12-$(OCH_3)_n$**, and polymer **6-$(OCH_3)_n$** show decreasing retention times, as expected for increasing hydrodynamic volumes (Figure 5; see also Figure 5s in the Supporting Information).

The weight-average molecular masses (M_w) for homologous **3-$(OCH_3)_{14}$**, **4-$(OCH_3)_{28}$**, **5-$(OCH_3)_{42}$** are ~4.9 kDa, ~10.5 kDa, and ~16 kDa, respectively; the polydispersities ($PD = M_w/M_n$) are in the 1.00–1.04 range, as expected for monodisperse oligomers. For these polyethers, the M_ws are overestimated (Table 4s in the Supporting Information); however, assuming that only about 75–80% of the injected mass of the polyether is eluted, good agreement with the formula masses is obtained. Similar discrepancies between the M_w and the formula mass were also observed for other polyarylmethyl polyethers.[18,19] In addition, admixtures of other polyethers, including those observed in FAB-MS, may contribute to these discrepancies between the M_ws and the formula masses. Using the assumption of 80% elution, the $M_w \approx 29$–33 kDa ($PD \approx 1.3$) for **6-$(OCH_3)_n$** may be corrected

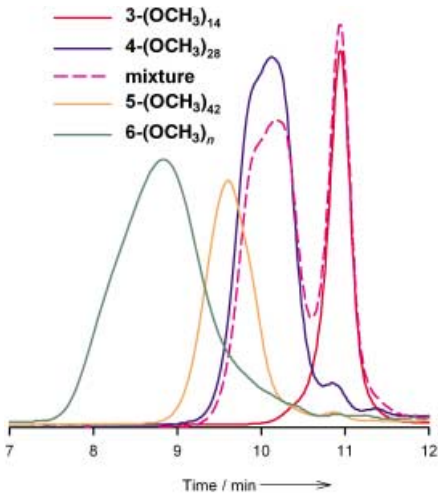

Figure 5. GPC chromatograms (refractive index detector) of **3-(OCH$_3$)$_{14}$**, **4-(OCH$_3$)$_{28}$**, **5-(OCH$_3$)$_{42}$**, polymer **6-(OCH$_3$)$_n$** and a mixture of **3-(OCH$_3$)$_{14}$** and **4-(OCH$_3$)$_{28}$**.

to $M_w \approx 26$ kDa. Similarly, $M_w \approx 14$ kDa is obtained for **12-(OCH$_3$)$_n$** after the correction; this M_w lies is between the formula mass for **5-(OCH$_3$)$_{42}$** and its higher homologue.[28]

The chromatograms for **3-(OCH$_3$)$_{14}$**, **4-(OCH$_3$)$_{28}$**, and **5-(OCH$_3$)$_{42}$** have distinct lineshapes, perhaps, reflecting distinct distributions of hydrodynamic shapes (and volumes) for mixtures of diastereomers. For **4-(OCH$_3$)$_{28}$** and **5-(OCH$_3$)$_{42}$**, additional small peaks (shoulders) are observed at the retentions times matching that of **3-(OCH$_3$)$_{14}$**. This is confirmed by the partially resolved chromatogram for a mixture of **3-(OCH$_3$)$_{14}$** and **4-(OCH$_3$)$_{28}$** (Figure 5).[29] Because the peak intensities in Figure 5 are proportional to the concentrations, **4-(OCH$_3$)$_{28}$** and **5-(OCH$_3$)$_{42}$** contain rather small admixtures of **3-(OCH$_3$)$_{14}$** (or compounds with similar hydrodynamic shapes/volumes). This suggests that the relatively intense peaks at $m/z \approx 3874$ in the FAB-MS of **4-(OCH$_3$)$_{28}$** and **5-(OCH$_3$)$_{42}$** arise from a relatively small amount of **3-(OCH$_3$)$_{14}$**. The ionization efficiency for this class of compounds decreases dramatically in relation to mass. This can result in the distortion in the relative intensities of the ions observed in the mass spectra.

Radii of gyration (R_g) for polyethers **4-(OCH$_3$)$_{28}$** and **5-(OCH$_3$)$_{42}$**, and polymer **6-(OCH$_3$)$_n$** in [D$_8$]THF are 1.7, 2.0, and 3.2 nm, respectively.[30]

Generation of polyradicals: Polyethers **3-(OCH$_3$)$_{14}$**, **4-(OCH$_3$)$_{28}$**, and **6-(OCH$_3$)$_n$** (0.8–1.2 mg per sample) were converted to the corresponding polyradicals **3**, **4**, and polymer **6**, respectively. The relevant chemistry and technical procedures are described elsewhere.[18,20] The samples of polyradicals in [D$_8$]THF (0.06–0.08 mL) were used for magnetic studies.

Magnetic studies: The results of magnetic studies are summarized in Tables 1 and 2 and Figures 6–10 (below).

For a typical sample of polyradical in [D$_8$]THF, magnetization (M) was measured as a function of magnetic field ($H = 0$–5×10^4 Oe at $T = 1.8$, 2.5, 3.5, 5, and 10 K) and temperature ($T = 1.8$–150 K at $H = 5000$, 500, 50 Oe). For selected samples, the following sequences of measurements were carried out: 1) without annealing (with sample chamber degassed at 90 K), 2) with prior annealing at 170 K (slightly above the melting point of the matrix), and 3) after exposure of the sample to room temperature for a short period (30–60 min). After completion of these measurements, the samples are kept at room temperature for about one month (or longer) to give effectively diamagnetic samples, which were used for point-by-point background correction for diamagnetism.

Numerical fitting of the curvature of low-temperature M versus H data ($T = 1.8$–5 K) to the Brillouin functions reveal relatively large values of average S, including $S \approx 18$ for polymer **6**. These fits provide average values of S (as the spin-weighed spin, S_s) and magnetization at saturation (M_{sat}).[31] As values of S and polydispersity of S increase along the homologous series of polyradicals, from annelated macrocycle **3** to polymer **6**, numerical fits require more variable parameters in the linear combination of the Brillouin functions. Greater values of S_s are associated with an increase in the number of unpaired electrons correlated ferromagnetically (or ferrimagnetically). The values of M_{sat} are reported per triarylmethyl site (more precisely, per triarylmethyl ether); the value of 1 μ_B would correspond to one unpaired electron per site. A fractional value of M_{sat}, that is, < 1 μ_B corresponds to a fraction of an unpaired electron per triarylmethyl site. Because M_{sat} is measured at low temperatures ($T = 1.8$–5 K), both antiferromagnetic interactions and chemical defects may contribute to its low values. In addition, the values of M_{sat}, which are based upon the weighed masses of polyethers, may be underestimated by incomplete mass transfers of polyethers and other mass losses during generation of polyradicals.[18]

For 14-radical **3**, adequate numerical fits to the M versus H data were obtained by using a single Brillouin function, with S and magnetization at saturation (M_{sat}) as two variable parameters; an approximate mean-field correction of the data for antiferromagnetic interactions ($\theta < 0$) significantly improves quality of the fit. The relatively small values of $|\theta|$, which are in the 0.1–0.2 K range, are required for the temperature-independent values of S and suggest the onset of weak antiferromagnetic interactions in the $T = 1.8$–5 K range.[32] The values of S obtained from such Brillouin plots, M/M_{sat} vs $H/(T-\theta)$, are in the 5.7–6.8 range (Table 1, Figure 6), below the value of $S = 7$ for 14 unpaired electrons coupled ferromagnetically. The values of $M_{sat} \approx 0.6$ μ_B per triarylmethyl site imply that about 60% of the unpaired electrons are present at low temperatures, though the values of average S are relatively high. It should be noted that samples of **3-(OCH$_3$)$_{14}$**, which were used for preparation of polyradicals **3**, contain various amounts of side products with higher molecular mass, as shown by relative amplitudes of peaks in FAB-MS (Table 1).

For the 28-radical **4**, numerical fits to the M versus H data were obtained by using linear combination of two Brillouin functions, $B(S_1)$ and $B(S_2)$, corresponding to the values of spin S_1 and S_2 [Eq. (1)]:

Table 1. Summary of magnetic data for tetradecaradical **3**.

3[a] sample	**3-(OCH$_3$)$_{14}$** sample	MS[b]	Mass [mg]	Anneal [K]	Brillouin S	Brillouin $-\theta$ [K]	Percolation S_s	Percolation $-\theta$ [K]	Percolation q	Percolation p	M_{sat}[c] [μ_B]	χT_{max}[d] [emu K mol^{-1}]	J/k [K]
1436	1351.Fpur	2–30	~1.2	170	6.5	0.2	–	–	–	–	–	–	11
1532	1431.2TLCsep	<2	1.08	170	5.9	0.1	5.9	0.1	0.66–0.67	0.89	0.60	15.7	15
				293	5.0	0.15	–	–	–	–	0.48	12.0	–
1566	1431.34high	10	0.80	90	6.8	0.07	6.6	0.0	0.59 –0.61	0.97 –1.00	0.60	17.7	10
				170	6.8	0.15	6.7	0.15	0.58 –0.61	0.99 –1.02	0.60	17.3	12
				293	5.2	0.15	–	–	–	–	0.49	11.4	–
1580	1431.2TLCfc	<2	0.91	170	5.7	0.1	5.7	0.1	0.67 –0.69	0.85 –0.87	0.59	14.5	13

[a] Yellow-green-brown color. [b] Relative peak amplitude for impurities in FAB-MS. [c] M_{sat} per mol of triarylmethyl ether. [d] χT_{max} per mol of polyether **3-(OCH$_3$)$_{14}$**.

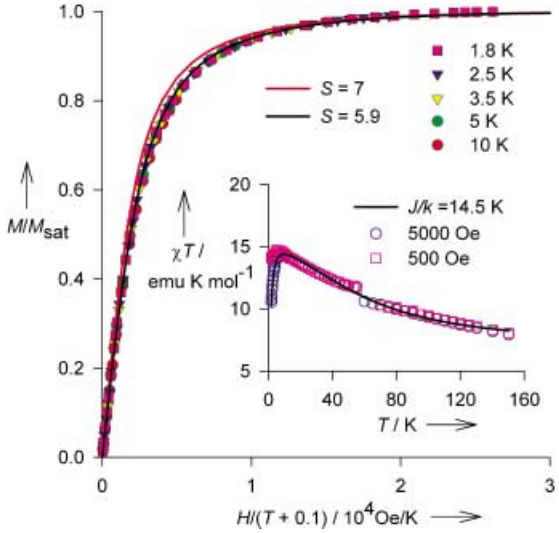

Figure 6. SQUID magnetometry for 14-radical **3** in [D$_8$]THF (sample label 1532, Table 1). Main plot: M/M_{sat} versus $H/(T-\theta)$. Solid lines correspond to the Brillouin functions with $S=7$ and $S=5.9$. The value of $S=5.9$ is obtained from a numerical fit by using Brillouin function with two variable parameters: $S=5.9$ and $M_{sat}=0.60\ \mu_B$ (parameter dependence of 0.30). Inset plot: χT versus T. The numerical fit to χT at $H=5000$ Oe for the square spin cluster of $S=6/2$–$1/2$–$6/2$–$1/2$ has two variable parameters $J/k=+14.5$ K and $N=1.46\times10^{-7}$ mol; parameter dependence is 0.57.

$$M = M_{sat}[(B(S_1) + w_2B(S_2)]/(1 + w_2) \quad (1)$$

The coefficient w_2 in Equation (1) depends on values of spin and molar fractions of the two spin systems. Four variable parameters were employed: M_{sat}, S_1, S_2, and w_2. Only numerical fits at $T=1.8$, 2.5, and 3.5 K were carried out to keep parameter dependence below 0.99 for each variable parameter. The values of spin-weighed average spin, $S_s=(S_1+w_2S_2)/(1+w_2)\approx10$, were obtained by using M/M_{sat} versus H/T functions. The values of M_{sat} are in the 0.5–0.6 μ_B range per triarylmethyl site (Figure 7, Table 2).

For polymer **6**, numerical fits to the M versus H data were obtained by using a linear combination of three Brillouin functions, $B(S_1)$, $B(S_2)$, and $B(S_3)$, corresponding to the values of spin S_1, S_2, and S_3 [Eq. (2)]:

$$M = M_{sat}[B(S_1) + w_2B(S_2) + w_3B(S_3)]/(1 + w_2 + w_3) \quad (2)$$

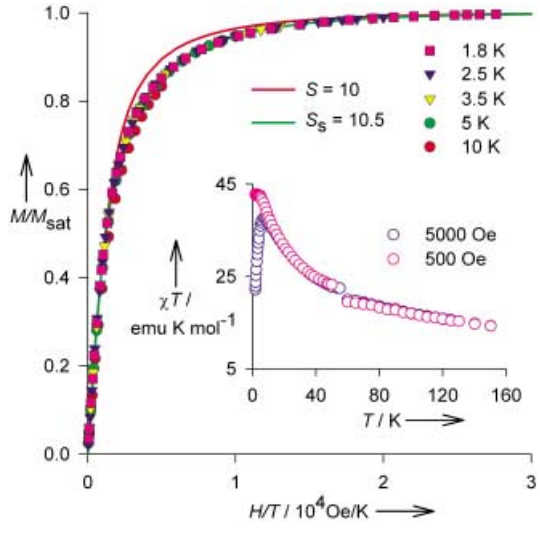

Figure 7. SQUID magnetometry for 28-radical **4** in [D$_8$]THF (sample label 1559, Table 2). Main plot: M/M_{sat} versus H/T. Solid line corresponds to numerical fit of the experimental data at 1.8 K by using the linear combination of two Brillouin functions [Eq. (1)], giving $S_s=10.5$; parameter dependencies for the four variable parameters are in the 0.57–0.99 range. Inset plot: χT versus T.

Table 2. Summary of magnetic data for polyradical **4** and polymer **6**.

Sample label	Mass[a] [mg]	Anneal [K]	S_s	M_{sat}[b] [μ_B]	χT_{max}[c] [emu K mol^{-1}]
polyradical **4**					
1559	1.08	170	10.5	0.54	45.3
1588	0.98	90	10.4	0.56	46.5
		170	10.4	0.56	47.0
		293	~1	0.08	1.3
polymer **6**					
1639	0.88	170	16.5	0.41	1.9
		293	dia	dia	dia[d]
1643	0.97	≤170	18.0	0.42	2.1
		293	dia	dia	dia
1678	1.10	≤170	19.1	0.64	3.4
		293	~4	0.17	0.2
1691[e]	0.88	≤170	~8	0.47	1.1
		293	~6	0.32	0.6
1708	1.04	≤170	~11	0.63	1.9

[a] Mass of polyethers **4-(OCH$_3$)$_{28}$** (sample label 1431.6xf) and **6-(OCH$_3$)$_n$** (sample label 1431.10TLC2x). [b] M_{sat} per mol of triarylmethyl ether. [c] For **4** and **6**, χT_{max} per mol of polyether **4-(OCH$_3$)$_{28}$** and triarylmethyl ether, respectively. [d] Nearly diamagnetic. [e] Dark grey-green color (for other samples of **4** and **6**, handled below 170 K, bright green color).

In Equation (2), one of the spin values, S_3, is set to 0.5 to account for the presence of $S=^1/_2$ impurities and to minimize the number of variable parameters. The third Brillouin function with relatively low value of spin is necessary to adequately reproduce the relatively slow approach to saturation for M versus H/T at high magnetic fields. With five variable parameters, M_{sat}, S_1, S_2, w_2, w_3, numerical fits at $T=1.8$ and 2.5 K were carried out. The values of $S_s=(S_1+w_2S_2+w_3S_3)/(1+w_2+w_3)$ are in the 17–19 range for the three best samples of **6**. (For the other two samples, $S_s\approx 8$ and 11 are obtained.) The values of M_{sat} are in the 0.4–0.6 μ_B range per triarylmethyl site (Figure 8).

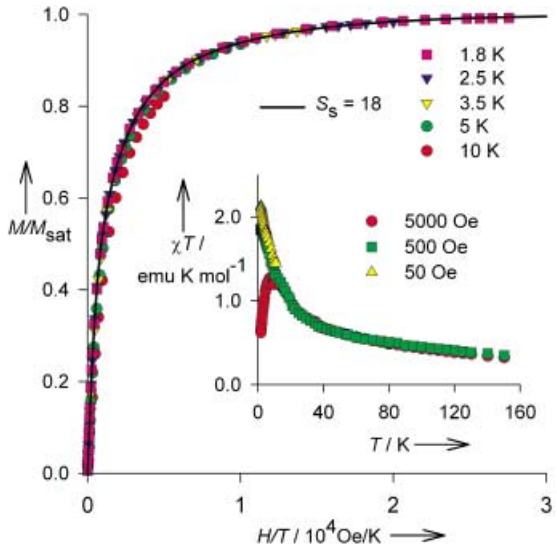

Figure 8. SQUID magnetometry for polymer **6** in [D_8]THF (sample label 1643, Table 2). Main plot: M/M_{sat} versus H/T. Solid line corresponds to numerical fit of the experimental data at 1.8 K by using the linear combination of three Brillouin functions [Eq. (2)], giving $S_s=18$; parameter dependencies for the five variable parameters are in the 0.76–0.98 range. Inset plot: χT versus T; χ is showed per mol of triarylmethyl ether.

The M versus T data at $H=5000$, 500, and/or 50 Oe are plotted as the product of magnetic susceptibility per mol of the starting polyether ($\chi=M/H$) and temperature versus temperature, that is, χT versus T for polyradicals **3**, **4**, and polymer **6** (insets in Figures 6–8). For all polyradicals, the values of χT increase with decreasing temperature from 150 K to about 5 K, indicating the thermal depopulation of the low-spin excited states. This behavior is consistent with the presence of a weak ferromagnetic coupling. In the $T=$ 1.8–5 K range, the downward turn in χT at modest magnetic fields (e.g., $H=5000$ Oe) is predominantly, if not exclusively, caused by the paramagnetic saturation. A small downward turn in χT is even found at low H for 14-radical **3**, which is consistent with weak antiferromagnetic interactions observed in the M/M_{sat} versus $H/(T-\theta)$ plots. However, the downward turns diminish at low H for **4**, and for **6** at 50 Oe, the χT rises with decreasing temperature down to 1.8 K. Most likely, intermolecular antiferromagnetic interactions are negligible for these larger polyradicals; this is consistent with their M/M_{sat} versus H/T plots.

The approximate ideal paramagnet behavior for **3** and **4** at low temperatures, found in the χT versus T plots, is compatible with the use of the Brillouin functions for the M versus H data. However, in polymer **6**, the χT versus T plots suggest the presence of very weak net ferromagnetic couplings.[33] Thus, the values of average spin $S_s\approx 18$ obtained from the M versus H/T plots (and numerical fits to the Brillouin functions) are only approximate, suggesting an effective ferromagnetic (or ferrimagnetic) correlation of about 36 electron spin.

The maximum values of χT for the plateau at low temperature (χT_{max}) are below those expected for the perfect polyradicals, that is, chemical defect-free and all unpaired electrons ferromagnetically coupled (Figures 6–8). This is not unexpected, as the values of S and M_{sat} are below those for the perfect polyradicals, as well. For **3** and **4**, $\chi T_{max}=15$–18 and 45–47 emu K mol^{-1} are obtained, respectively. For monodisperse $S=7$ and $S=14$ polyradicals, $S(S+1)/2=28$ and 105 emu K mol^{-1} should be obtained, respectively. For polymer **6**, $\chi T_{max}=2$–3 emu K mol^{-1}, calculated per mol of triarylmethyl ether ($M_w=278.97$) is obtained for the best three samples with $S=17$–19.

14-Radical **3** may be viewed as an organic spin cluster of four component spins, $S=6/2$–$1/2$–$6/2$–$1/2$, arranged on the vertices of a square, in which all four nearest neighbor pairwise exchange couplings (J/k) through the biphenylene coupling units are identical.[19] Energy eigenvalues for Heisenberg Hamiltonian for this spin tetramer are determined by the vector decoupling technique.[34] Equations for magnetization, including saturation effects were derived using standard formulas.[4] Experimental data for the χT versus T plots were fit as MT versus T. At $H=5000$ Oe, two variable parameters, J/k (identical for all nearest neighbors) and N (number of moles of polyradical), were used [Eqs. (1s)–(3s) and Table 5s in the Supporting Information]. For all-ferromagnetic and all-antiferromagnetic couplings, $J/k=+12\pm 3$ K and $J/k=-9\pm 2$ K, respectively, were obtained. The fits with the $J/k>0$ model provide smaller norms (by factor of 2–5), relative to those for the $J/k<0$ model. Analogous numerical fits at lower magnetic field ($H=500$ Oe) require two additional variable parameters: the mean-field parameter θ ($\theta<0$), to account for weak antiferromagnetic interactions (probably intermolecular) and numerical correction for diamagnetism (M_{dia}).[35] However, neither the $J/k>0$ model nor the $J/k<0$ model is consistent with the Brillouin fits to the magnetic-field dependence of magnetization. In the absence of chemical defects, the $J/k>0$ model should give $S=7.0$ and $M_{sat}=1.0$ μ_B. Analogously, the $J/k<0$ model, should give $S=5.0$ and $M_{sat}=5/7$ $\mu_B\approx 0.71$ μ_B. Most likely, chemical defects and mixture of conformations with distribution of J/k would have to be taken into account. Such numerical fits of the χT versus T data would require too many variable parameters versus the relatively low information content of the χT versus T curves.

An alternative model involves the numerical fit of the M versus H data at low temperatures. Assuming that most of the nearest neighbor exchange couplings are significant, that is, $|J/k|$ greater than few Kelvin, the Brillouin functions (corrected with mean-field parameters, as necessary for **3**),

provide good approximation for M at low temperatures $T \leq 5$ K. The previously developed percolation model was adapted to the organic spin tetramer corresponding to the 14-radical **3**.[19] The variable parameters q and p are defined as follows: 1) probabilities for ferromagnetic ($J>0$) and antiferromagnetic ($J<0$) coupling through each biphenylene coupling unit are q and $1-q$, respectively; 2) probabilities for an unpaired electron and a chemical defect at a triarylmethyl site are p and $1-p$, respectively. In regard to parameter p, only spin systems at the two 4-biphenyl-substituted sites are explicitly enumerated; chemical defects at the other twelve sites are accounted for, approximately, by scaling their contribution to spin with a factor of p.[36] Overall, 15 configurations, with 0–4 antiferromagnetic ($J<0$) couplings through biphenylene coupling units and 0–2 chemical defects at the 4-biphenyl-substituted sites, are considered. Each enumerated spin system, with r ferromagnetic ($J>0$) biphenylene coupling units and s chemical defects, enters into the linear combination of the Brillouin functions with a factor of $b_{r,s}=[q^r(1-q)^{4-r}][ps(1-p)^{2-s}]$.[19]

Numerical fits to the mean-field corrected M versus $H/(T-\theta)$ data give $p=0.9$–1.0 and $q=0.6$–0.7, that is, low density of chemical defects and predominantly ferromagnetic couplings are found (Figure 9).[37] Values of S_s calculated

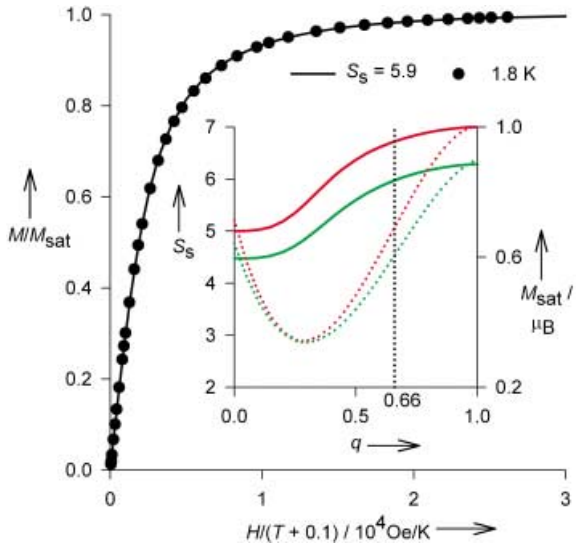

Figure 9. SQUID magnetometry for 14-radical **3** in [D_8]THF (sample label 1532, Table 1). Main plot: M/M_{sat} versus $H/(T-\theta)$. Solid line corresponds to numerical fit of the experimental data at 1.8 K by using the percolation model with two variable parameters, $p=0.89$ and $q=0.66$ (parameter dependence of 0.99); these values of p and q correspond to $S_s=5.9$. Inset plot: plot of S_s (solid lines) and M_{sat} (dotted lines) versus q (fraction of ferromagnetic couplings through 3,4′-biphenylene) for $p=1.0$ (red lines) and $p=0.9$ (green lines), as calculated from the percolation model for 14-radical **3**. The vertical black, dotted line shows $q=0.66$; its crossing points with the green lines give approximate values of S_s and M_{sat} for this sample.

from parameters p and q are similar to those obtained from simple Brillouin fits. Most importantly, this two-parameter fit gives values of M_{sat} that are in quantitative agreement with the experiment (Table 1).

Alternative numerical fits, which include the mass of the polyether (m) as variable parameter, were attempted. The two-parameter (p and m) fits give significantly greater norms than those in Table 1. However, the three-parameter (p, q, and m) fits are overparametrized; the optimized values of m are typically 50% greater than the weighed mass of polyethers. Also, the optimized values of $q \approx 0.4$ would suggest that the antiferromagnetic interactions ($J<0$) are relatively important; in contrast, the MT versus T fits have lower norms for the $J<0$ model, relative to the $J>0$ model. Therefore, within the approximations of our models, the weighed masses of 14-ether **3-(OCH$_3$)$_{14}$** (Table 1) are probably adequate for calculation of number of moles of 14-radical **3**.

The inset of Figure 9 illustrates the behavior of S_s and M_{sat} within our percolation model. For $p=1.0$ (no chemical defects), S_s as a function of q varies between $S_s=5$ ($q=0$, all-antiferromagnetic couplings) to $S_s=7$ ($q=1.0$, all-ferromagnetic couplings). For M_{sat}, a minimum value of $M_{sat}(\min)\approx 0.34$ is found at $q(\min)\approx 0.28$; at this value of q, $S_s\approx 5.47$ is obtained. For $p=0.9$ (and $p=0.8$, not shown), the S_s and M_{sat} are shifted to somewhat lower values; however, for $q(\min)\approx 0.3$, $M_{sat}(\min)$ has similar value in the $p=0.8$–1.0 range. When antiferromagnetic coupling is dominant but not exclusive, relatively large values of S_s are still possible, even with as little as ~1/3 of unpaired electrons remaining at low temperature. Also, the relative values of S_s and M_{sat} may provide a qualitative measure of the relative contributions of ferromagnetic and antiferromagnetic couplings for polyradicals with low density of chemical defects.

Thermal stability (persistence) of polyradicals: Annealing at 170 K (just above the melting point of the matrix) for a few minutes does not affect the results for samples of **3** and **4**. (Only one sample of each polyradical was studied.) Selected samples of polyradicals were also studied following annealing at room temperature for about 0.5 h. For polymer **6**, two samples became diamagnetic and the other two samples had $S_s=4$–6 after about 0.5 h at room temperature (Table 2). For 28-radical **4**, $S_s\approx 1$ was obtained for one studied sample. 14-Radical **3** possesses remarkable stability; for two samples after 0.5 h at room temperature, the values of S were reduced from 6.8 to 5.2 and 5.9 to 5.0. Moreover, the M_{sat} values were reduced to about 80% of their original values (Figure 10, Table 1). Thus, 14-radical **3** may be viewed as persistent at room temperature. The variations in apparent thermal persistence of **3**, **4**, and **6** may result from not only their structural differences, but also the different degree of oxidation (e.g., excess of iodine reacting with radicals at higher temperature) for each sample. After being kept at room temperature for one month (or longer), all reported samples of **3**, **4**, and **6** had become effectively diamagnetic.

Conclusion

The studied annelated macrocyclic polyradicals **3** and **4** show average values of S of about 5.7–6.8 and 10, respec-

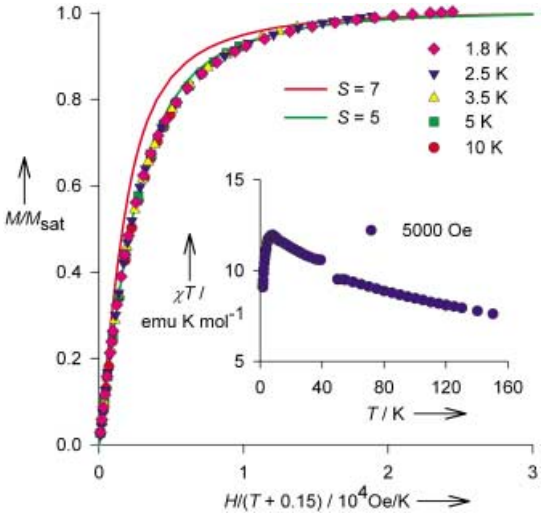

Figure 10. SQUID magnetometry for 14-radical **3** in [D_8]THF after annealing for 0.5 h at room temperature (sample label 1532, Table 1). Main plot: M/M_{sat} versus $H/(T-\theta)$. Solid lines correspond to the Brillouin functions with $S=7$ and $S=5$. Inset plot: χT versus T.

tively. The polymer **6** has average S of about 18. The values of S and molar fractions of unpaired electrons at low temperatures (M_{sat}) suggest that ferromagnetic couplings predominate in polyradicals **3** and **4**, though there are substantial antiferromagnetic couplings present.

Based upon the one mode of annelation for calix[4]arene-based macrocycles studied in this work, polymer **1** is likely to possess significant content of annelated macrocyclic structures with fractal dimensionality beyond one. Furthermore, these annelated macrocyclic structures may contribute to the predominant ferromagnetic couplings and large net values of S found in polymer **1**. Because the other modes of annelation for polymer **1** remain unexplored, the present results provide only partial rational for magnetic ordering in polymer **1**.

Experimental Section

Gel permeation chromatography and multiangle light scattering (GPC/MALS) studies: A 17-Angle light scattering detector (Wyatt DAWN EOS) and an interferometric refractive index detector (Wyatt Optilab DSP) were used for GPC/MALS studies. One or two 4.6×300 mm 5 μ Phenogel GPC columns (500 Å or following in sequence 10^3 Å), with THF as a mobile phase, were used. The flow rate of THF was 0.4 or 0.5 mL min^{-1} and dn/dc was computed on-line. A solution of oligomer or polymer in THF (100 μL) was injected into 20 μL loop, typically, three times.

General procedures for syntheses and polymerizations: All glassware was connected to vacuum lines with solv-seal joints and flexible connectors (stainless steel or Teflon). A weighed amount of polyether was placed in a Schlenk vessel (equipped with Kontes or Chemglass high-vac Teflon stopcock). The Schlenk vessel with the polyether (and magnetic stir bar) was evacuated overnight while immersed in a 70 °C oil bath. While the Schlenk vessel with polyether was allowed to attain room temperature, the vacuum line was heated with heat gun prior to vacuum transfer of solvent (THF or diethyl ether). After solvent was transferred and all polyether dissolved, solution of *n*BuLi or *t*BuLi was added at −78 °C under argon gas flow. After a specified time/temperature sequence, the formed aryllithium compound was treated with additional reagents. All isolated products with an estimated mass of less than about 20 mg were evaporated into small vials for weighing on analytical balance. In the NMR data EM is exponential multiplication and GB is Gaussian broadening. In the MS data NBA = 3-nitrobenzylalcohol, ONPOE = (*o*-nitrophenyl)octylether, and % RA is % relative amplitude.

Compound 8-$(OCH_3)_8Br_2$ and side product 10-$(OCH_3)_{15}Br_2$: *t*BuLi (0.50 mL of a ~1.5 M solution in pentane, 0.75 mmol) was added to a solution of **7-$(OCH_3)_6Br_2$** (0.300 g, 0.168 mmol) in THF (8.50 mL) in a heavy-wall Schlenk vessel at −78 °C. After 2 h, the reaction mixture was warmed up to −20 °C for 10 min, and then re-cooled to −78 °C. Following addition of $ZnCl_2$ (0.44 mL of 0.80 M solution in diethyl ether, 0.354 mmol), the reaction mixture was allowed to attain ambient temperature for 3 h. The resultant clear yellow solution was transferred to a glovebox. [$Pd(PPh_3)_4$] (13.0 mg, 0.0101 mmol) and racemate **9** (0.270 mg, 0.505 mmol) were added to the reaction mixture. Subsequently, the reaction mixture was heated at 100 °C for 1.5 days. After extraction with diethyl ether, the organic layer was dried over $MgSO_4$ and concentrated in vacuo to give a brown solid. Column chromatography (TLC grade silica gel, 2.5–5 % diethyl ether in hexane), followed by the treatment with diethyl ether/MeOH, gave 232 mg (56 %) of white powder of **8-$(OCH_3)_8Br_2$** and 14.3 mg (4 %) of white powder of **10-$(OCH_3)_{15}Br_2$**.

Another reaction on the same scale gave 186 mg (45 %) of white powder of **8-$(OCH_3)_8Br_2$** and 14.3 mg (3 %) of white powder of **10-$(OCH_3)_{15}Br_2$**, respectively.

Compound 8-$(OCH_3)_8Br_2$: Softened at 211 °C, m.p. 216–219 °C; FABMS (3-NBA) cluster: m/z (% RA for m/z = 400–5200) for $[M-OCH_3]^+$: 2406.2 (39), 2407.2 (53), 2408.2 (86), 2409.2 (100), 2410.2 (95), 2411.2 (74), 2412.2 (51), 2413.2 (30), 2414.2 (15); calcd for $C_{163}H_{179}O_7Br_2$ $[M-OCH_3]^+$: 2406.2 (21), 2407.2 (39), 2408.2 (77), 2409.2 (88), 2410.2 (100), 2411.2 (84), 2412.2 (55), 2413.2 (29), 2414.2 (12); IR: $\tilde{\nu}$ = 1592 (Ar), 1078 cm^{-1} (C-O-C).

^{1}H NMR (500 MHz, EM = −1.60, GB = 0.90, C_6D_6, 293 K): δ = 8.083 (br t, 2H), 8.034, 8.032 (2t, J = 2, 2 Hz, 1H), 7.995 (t, J = 2 Hz, 1H), 7.983 (t, J = 2 Hz, 2H), 7.865 (br s, J = 2 Hz, 2H), 7.821 (br s, 1H), 7.796 (br s, 1H), 7.774 (t, J = 2 Hz, 1H), 7.630 (d, J = 9, 2H), 7.13–7.60 (m, 55H), 3.070 (br s, 3H), 2.969, 2.967 (2s, 3H) diastereomer, 2.918, 2.914 (s, br s, 9H), 2.909 (s, 3H), 2.901, 2.899 (2s, 6H), 1.228, 1.226 (2s 18H), 1.186 (s, 9H), 1.171 (s, 9H), 1.163 (s, 9H), 1.156 (s, 9H), 1.152 (s, 9H), 1.143 (s, 9H), 1.134 (s, 9H), 1.122 ppm (s, 9H); ^{1}H NMR (500 MHz, EM = −1.60, GB = 0.90, [D_6]benzene, 328 K): δ = 8.038–8.020 (m, 3H), 7.974, 7.971 (2t, J = 2, 2 Hz, 2H), 7.905 (t, J = 2 Hz, 1H), 7.788 (t, J = 2 Hz, 1H), 7.752–7.768 (m, 3H), 7.718 (t, J = 2 Hz, 1H), 7.591 (d, J = 8 Hz, 2H), 7.137–7.521 (m, 55H), 3.072 (s, 3H), 2.963 (s, 3H), 2.932, 2.928 (2s, 9H), 2.918, 2.915 (2s, 6H), 2.910 (s, 3H), 1.230 (s, 18H), 1.191 (s, 9H), 1.178 (s, 9H), 1.172 (s, 9H), 1.161 (s, 9H), 1.157 (s, 9H), 1.153 (s, 9H), 1.147 (s, 9H), 1.130 ppm (s, 9H).

^{1}H NMR (500 MHz, EM = −1.40, GB = 0.90, [D_6]benzene, 348 K, ^{1}H–^{1}H COSY cross-peaks in aromatic region): 1,3,5-Trisubstituted benzene rings (rings A - D): Ring A: δ = 8.116, 8.014 (2t, J = 2, 2 Hz, 1H, 7.966, 7.693), 7.966 (t, J = 2 Hz, 1H, [8.116, 8.014], 7.693), 7.693 ppm (t, J = 2 Hz, 1H, [8.116, 8.014], 7.966); Ring B: δ = 8.003, 8.002 (2t, J = 2, 2 Hz, 1H, 7.956, 7.728), 7.956 (t, J = 2 Hz, 1H, [8.003, 8.002], 7.728), 7.728 ppm (t, J = 2 Hz, 1H, [8.003, 8.002], 7.956); Ring C: δ = 7.987 (t, J = 2 Hz, 1H, 7.861, 7.404), 7.861 (t, J = 2 Hz, 1H, 7.987, 7.404), 7.404 ppm (t, J = 2 Hz, 1H, 7.861, 7.861); Ring D: δ = 7.745 (t, J = 2 Hz, 1H, 7.734, 7.687), 7.734 (t, J = 2 Hz, 1H, 7.745, 7.687), 7.687 ppm (t, J = 2 Hz, 1H, 7.745, 7.734); 1,4-disubstituted benzene rings (rings 1–14): δ = 7.570 (d, J = 9 Hz, 2H, 7.239), 7.239 (d, J = 9 Hz, 2H, 7.570), 7.494 (d, J = 9 Hz, 2H, 7.190), 7.190 (d, J = 9 Hz, 2H, 7.494), 7.489 (d, J = 9 Hz, 2H, 7.218), 7.218 (d, J = 9 Hz, 2H, 7.489), 7.481 (d, J = 9 Hz, 2H, 7.195), 7.195 (d, J = 9 Hz, 2H, 7.481), 7.468 (d, J = 8 Hz, 2H, 7.336), 7.336 (d, J = 8 Hz, 2H, 7.468), 7.438 (d, J = 9 Hz, 2H, 7.185), 7.185 (d, J = 9 Hz, 2H, 7.438), 7.432 (d, J = 9 Hz, 2H, 7.367), 7.367 (d, J = 9 Hz, 2H, 7.432), 7.406 (d, J = 9 Hz, 2H, 7.178), 7.178 (d, J = 9 Hz, 2H, 7.406), 7.396 (d, J = 9 Hz, 2H, 7.175), 7.175 (d, J = 9 Hz, 2H, 7.396), 7.374 (d, J = 9 Hz, 2H, 7.275), 7.275 (d, J = 9 Hz, 2H, 7.374), 7.372 (d, J = 9 Hz, 2H, 7.146), 7.146 (d, J = 9 Hz, 2H, 7.372), 7.361 (d, J = 9 Hz, 2H, 7.268), 7.268 (d, J = 9 Hz, 2H, 7.361), 7.260 (s, 4H, overlapped AB), 7.249, 7.248 ppm (s, 2H, 2H, overlapped AB); aliphatic region: δ = 3.076 (s, 3H), 2.963 (s, 3H), 2.946 (s, 3H), 2.942 (s, 6H), 2.927 (s, 3H), 2.918 (s, 6H), 1.234 (s, 9H), 1.232 (s, 9H), 1.197 (s, 9H), 1.184 (s, 9H),

1.181 (s, 9H), 1.170 (s, 9H), 1.162 (s, 18H), 1.157 (s, 9H), 1.139 ppm (s, 9H).

$^{13}C\{^1H\}$DEPT(135°)NMR (125 MHz, EM = −0.90/-0.70, GB = 0.90/0.40, [D_6]benzene, 293 K): aromatic quaternary region, expected: 40 resonances; found: 30 resonances at δ = 150.38 (q), 150.28 (q), 150.25 (q), 150.20 (q), 150.00 (q), 149.92 (q), 149.87 (q), 149.81 (q), 149.76 (q), 146.8 (q), 146.6 (q), 146.0 (q), 145.1 (q), 144.9 (q), 144.6 (q), 144.0 (q), 143.7 (q), 143.01 (q), 142.95 (q), 142.86 (q), 142.42 (q), 142.39 (q), 141.5 (q), 141.22 (q), 141.17 (q), 141.07 (q), 140.8 (q), 140.4 (q), 140.2 (q), 121.6 ppm (q); aromatic non-quaternary region, expected: 40 resonances; found: 27 resonances at δ = 131.5, 131.05, 131.02, 130.11, 130.07, 130.02, 129.88, 129.74, 129.70, 129.58, 129.48, 129.3, 129.2, 128.7 ([D_5H]benzene), 128.3, 127.30, 127.27, 127.0, 126.6, 126.4, 126.2, 125.5, 125.39, 125.33, 125.26, 125.20, 125.17, 125.13 ppm; aliphatic region, δ = 88.28 (q), 88.21 (q), 88.1 (q), 87.8 (q), 87.7 (q), 87.1 (q), 52.68, 52.65, 52.59, 52.55, 52.51, 52.48, 52.3, 34.81 (q), 34.75 (q), 34.72 (q), 31.85, 31.82, 31.80, 31.74 ppm.

Compound 10-$(OCH_3)_{15}Br_2$: FABMS (ONPOE) cluster: *m*/*z* (% RA for *m*/*z* = 1000–6200) for $[M-OCH_3]^+$: 4358.3 (38), 4359.3 (63), 4360.3 (82), 4361.3 (98), 4362.4 (100), 4363.3 (92), 4364.3 (69), 4365.3 (50), 4366.4 (29), 4367.3 (20); calcd for $C_{303}H_{337}O_{14}Br_2$ $[M-OCH_3]^+$: 4358.4 (17), 4359.4 (38), 4360.4 (66), 4361.4 (89), 4362.4 (100), 4363.4 (94), 4364.4 (75), 4365.4 (51), 4366.4 (30), 4367.4 (16), 4368.4 (7).

^1H NMR (500 MHz, EM = −1.20, GB = 0.90, [D_6]benzene, 293 K): δ = 7.10–8.05 (m, 124H), 2.89–3.10 (45H), 1.11–1.27 ppm (171H); ^1H NMR (500 MHz, EM = −1.20, GB = 0.90, [D_6]benzene, 328 K): δ = 7.10–8.05 (m, 148H; expected 124H), 2.89–3.10 (45H), 1.11–1.27 ppm (161H; expected 171H).

^1H NMR (500 MHz, EM = −1.20, GB = 0.90, [D_6]benzene, 348 K, ^1H-^1H COSY cross-peaks in aromatic region) 1,3,5-trisubstituted benzene rings (rings A,A′–D,D′); ring A: δ8.060 (br, 1H, 7.989, 7.633), 7.989 (brs, 1H, 8.060, 7.633), 7.633 ppm (brs, 1H, 8.060, 7.989); ring A′: δ = 7.997 (br, 1H, 7.857, 7.382), 7.857 (t, 1H, 7.997, 7.382), 7.382 ppm (br, 1H, 7.997, 7.857); ring B: δ = 8.020 (t, *J* = 2, 1H, missing, 7.674), 7.994 (br, 1H, missing, 7.674),7.674 ppm (t, *J* = 2, 1H, 8.020, 7.994); ring B′: δ = 8.017 (t, *J* = 2, 1H, 7.969, 7.691), 7.969 (t, *J* = 2, 1H, 8.017, 7.691), 7.691 ppm (t, *J* = 2, 1H, 8.017, 7.969); ring C: δ = 7.997 (brs, 1H, 7.946, 7.754), 7.946 (t, *J* = 2, 1H, 7.997, 7.754), 7.754 ppm (brt, *J* = 2, 1H, 7.997, 7.946); ring C′: δ = 7.793, 7.783 (t, t, *J* = 2, *J* = 2, 1H, 7.699, 7.671), 7.699 (br, 1H, [7.793, 7.783], 7.671), 7.671 ppm (t, *J* = 2, 1H, [7.793, 7.783], 7.699); ring D: δ = 7.973 (t, *J* = 2, 1H, 7.854, 7.387), 7.854 (t, *J* = 2, 1H, 7.973, 7.387), 7.387 ppm (br, 1H, 7.973, 7.854); ring D′: δ = 7.757 (br, 1H, 7.737, 7.699), 7.737 (br, 1H, 7.757, 7.699), 7.699 (br, 1H, 7.757, 7.737); 1,4-disubstituted benzene rings (rings 1–25): δ = 7.579 (d, *J* = 9, 4H), 7.14–7.51 ppm (m, 96H); aliphatic region: expected 15 resonances for the methoxy groups; found 22 resonances (45H): δ = 3.093, 3.087 (brs, s, 4.53H), 3.079 (s, 0.51H), 3.025, 3.022, 3.019 (3s, 1.25H), 3.006, 3.003, 2.999 (3s, 2.07H), 2.993, 2.986, 2.982, 2.978, 2.975 (brs, 4s, 5.13H), 2.966, 2.964, 2.961, 2.957, 2.949 (4s, brs, 18.48H), 2.932 (brs, 9.89H), 2.921 (s, 1.15H), 2.912 ppm (s, 1.99H); expected 19 resonances for the *tert*-butyl groups; found 14 singlets and 1 multiplet (171H): δ = 1.253–1.262 (m, 8.35H), 1.235, 1.233 (2s, 18.81H), 1.201, 1.198 (brs, s, 19.60H), 1.187, 1.183 (2brs, 37.98H), 1.175, 1.169, 1.167, 1.162, 1.158 (3brs, 2s, 69.68H), 1.154 (s, 3.33H), 1.150 (s, 3.76H), 1.143 ppm (s, 9.49H).

Annelated macrocyclic polyethers 3-$(OCH_3)_{14}$, 4-$(OCH_3)_{28}$, 5-$(OCH_3)_{42}$, 12-$(OCH_3)_n$ and polymer 6-$(OCH_3)_n$: *t*BuLi (0.22 mL of a ~1.5 M solution in pentane as 37 drops, 0.329 mmol) was added to a solution of **7-$(OCH_3)_6Br_2$** (136 mg, 0.0761 mmol) in THF (5.6 mL) in a heavy-wall Schlenk vessel at −78 °C. After 2.5 h, the reaction mixture was warmed up to −20 °C for 15 min, and then re-cooled to −78 °C. Following addition of $ZnCl_2$ (0.17 mL of 0.96 M solution in diethyl ether, 0.165 mmol), the reaction mixture was allowed to attain ambient temperature for 2.5 h. The resultant clear yellow solution was transferred to a glovebox. [$Pd(PPh_3)_4$] (6.5 mg, 0.0056 mmol) and **8-$(OCH_3)_8Br_2$** (186 mg, 0.0761 mmol) were added to the reaction mixture. Subsequently, the reaction mixture was heated at 100 °C for 2 days. After extraction with diethyl ether, the organic layer was dried over $MgSO_4$ and concentrated in vacuo to give a clear solid (0.306 g). The greater part of this clear solid (0.302 g) was filtered through TLC grade silica gel (300 mL) with 20% diethyl ether in hexane to give 294.8 mg of the crude product. Column chromatography (TLC grade silica gel, 5–20% diethyl ether in hexane) using 0.28 g of the crude product, gave ten fractions according to decreasing R_f values. FAB-MS (ONPOE) was used extensively to analyze these fractions and to monitor their purification; selected spectra are summarized in Tables 1s, 2s, and 3s (see the Supporting Information) for this reaction (and another reaction). Sample numbers are provided for one-to-one correlation between the described samples, their FAB-MS, and the corresponding polyradicals.

Fraction 2: Two PTLC separations (silica gel, 7% diethyl ether in hexane, developed twice) gave 17.6 mg (5.9%) of white powder of **3-$(OCH_3)_{14}$** (sample label 1431.2TLCsep, used for preparation of SQUID sample); subsequently, part of this sample was filtered and treated with MeOH (and MeOH/diethyl ether) to give 6.6 mg of white solid (sample label 1431.2TLCfc, used for preparation of SQUID sample).

Fractions 3 and 4 (combined): PTLC (silica gel, 7% diethyl ether in hexane, developed twice) gave two sub-fractions: high R_f, 14.5 mg, which after additional PTLC gave 6.3 mg of white powder of **3-$(OCH_3)_{14}$** (sample label 1431.34 high, used for preparation of SQUID sample); low-R_f 1.6 mg of white powder of **4-$(OCH_3)_{28}$** (sample label 1431.34). Neither of the samples were included in the overall yields because of significant amount of impurities detected by FAB-MS (Tables 1s and 2s, in the Supporting Information).

Fraction 5: Treatment with MeOH gave 5.3 mg of **4-$(OCH_3)_{28}$** (sample label 1431.5x).

Fraction 6: Treatment with MeOH gave 20.2 mg of **4-$(OCH_3)_{28}$** (sample label 1431.6x); subsequently, part of this sample was filtered and treated with MeOH/diethyl ether to give 15.1 mg of white solid (sample label 1431.6xf, used for preparation of SQUID samples).

Fraction 7: Treatment with MeOH gave 3.6 mg of **5-$(OCH_3)_{42}$** (sample label 1431.7x).

Fraction 8: Treatment with MeOH gave 16.5 mg of **5-$(OCH_3)_{42}$** (sample label 1431.8x)

Fraction 9: Treatment with MeOH gave 17.6 mg (6.5%) of **12-$(OCH_3)_n$** (sample label 1431.9x).

Fraction 10: PTLC (silica gel, 12% diethyl ether in hexane), followed by treatment with MeOH gave 93.6 mg (31%) of white powder of **6-$(OCH_3)_n$** (sample labels: 1431.10TLCx and 1431.10TLC2x, used for preparation of SQUID samples).

A second polymerization was carried on the 0.02 mmol scale (36.6 mg of **7-$(OCH_3)_6Br_2$**) with a couple minor differences in the reaction conditions: the reaction mixture was warmed up to −20 °C for 2 h following the addition of *t*BuLi and the reaction mixture was kept at 100 °C for 3 days before work up. Isolated amounts and FAB-MS for six chromatographic fractions containing **3-$(OCH_3)_{14}$** obtained from this reaction are summarized in Table 1s (Supporting Information: sample labels starting with 1351). Overall yield for **3-$(OCH_3)_{14}$** was 9.1 mg (~12%, sample labels: 1351Dsep, 1351Esep, 1351F), though the purity, as suggested by FAB-MS, was not as good as for **3-$(OCH_3)_{14}$** from the large-scale reaction. The chromatographic fractions containing higher homologues of **3-$(OCH_3)_{14}$** were relatively impure and are not reported.

Compound 3-$(OCH_3)_{14}$: Overall yield: 17.6 mg (5.9%) (sample label 1431.2TLCsep); softening at 256 °C, m.p. 270–272 °C; FABMS (ONPOE) wide range scan: *m*/*z* (% RA for *m*/*z* = 1600–8500): 1922 (6) $[M-2OCH_3]^{2+}$, 3874 (100) $[M-OCH_3]^+$, 5498 (1.5); narrow range scan: *m*/*z* (% RA for *m*/*z* = 1917–1927) for $[M-2OCH_3]^{2+}$: 1919.6 (30), 1920.1 (53), 1920.6 (72), 1921.1 (100), 1921.6 (85), 1922.1 (69), 1922.6 (42), 1923.1 (27), 1923.6 (17); calcd for $C_{278}H_{310}O_{12}$ $[M-2OCH_3]^{2+}$: 1920.2 (20), 1920.7 (60), 1921.2 (95), 1921.7 (100), 1922.2 (80), 1922.7 (50), 1923.2 (26), 1923.7 (12); narrow range scan: *m*/*z* (% RA for *m*/*z* = 3805–3895) for $[M-OCH_3]^+$: 3870.4 (27), 3871.4 (47), 3872.4 (78), 3873.4 (100), 3874.4 (91), 3875.4 (77), 3876.4 (48), 3877.4 (27); calcd for $C_{279}H_{313}O_{13}$ $[M-OCH_3]^+$: 3871.4 (19), 3872.4 (60), 3873.4 (95), 3874.4 (100), 3875.4 (79), 3876.4 (50), 3877.4 (27), 3878.4 (12), 3879.4 (5); narrow range scan *m*/*z* (% RA for *m*/*z* = 5340–5580) for impurity $C_{395}H_{449}O_{19}$ $[M-OCH_3]^+$: 5497.5 (100); calcd for $C_{395}H_{449}O_{19}$ $[M-OCH_3]^+$: 5496.4 (6), 5497.4 (27), 5498.4 (60), 5499.4 (89), 5500.4 (100), 5501.4 (90), 5502.4 (67), 5503.4 (44), 5504.4 (25), 5505.4 (12), 5506.4 (5); IR: $\tilde{\nu}$ = 1594 (Ar), 1078 cm^{-1} (C-O-C); ^1H NMR (500 MHz, [D_6]benzene, 293 K): δ = 6.70–8.60 (m, 112H), 2.20–3.30 (m, 42H), 0.70–1.50 ppm (m, 162H).

Compound 4-$(OCH_3)_{28}$: Overall yield: 25.5 mg (8.6%) (sample labels: 1431.5x and 1431.6x); softening at 216°C, m.p. 233–235°C; FABMS (ONPOE) wide range scan (label 1431.6x): *m/z* (% RA for *m/z* = 3400–13600): 3874 (100), 6155 (10), 7779 (67) $[M-OCH_3]^+$; narrow range scan (label 1431.6x): *m/z* (% RA for *m/z* = 3805–3890) for $C_{279}H_{313}O_{13}$ $[M-C_{281}H_{319}O_{15}]^+$: 3870.3 (32), 3871.3 (52), 3872.3 (100), 3873.3 (96), 3874.3 (96), 3875.3 (70), 3876.3 (51), 3877.3 (32); narrow range scan (label 1431.6xf): *m/z* (% RA for *m/z* = 3868–3879) for $C_{279}H_{313}O_{13}$ $[M-C_{281}H_{319}O_{15}]^+$: 3870.3 (31), 3871.3 (50), 3872.4 (75), 3873.3 (100), 3874.3 (92), 3875.3 (74), 3876.3 (48), 3877.3 (31); narrow range scan (label 1431.5x): *m/z* (% RA for *m/z* = 3863–3883) for $C_{279}H_{313}O_{13}$ $[M-C_{281}H_{319}O_{15}]^+$: 3870.3 (25), 3871.4 (43), 3872.3 (77), 3873.3 (99), 3874.4 (100), 3875.3 (74), 3876.3 (48), 3877.3 (33); calcd for for $C_{279}H_{313}O_{13}$ $[M-C_{281}H_{319}O_{15}]^+$: 3871.4 (19), 3872.4 (60), 3873.4 (95), 3874.4 (100), 3875.4 (79), 3876.4 (50), 3877.4 (27), 3878.4 (12), 3879.4 (5); narrow range scan (label 1431.34): *m/z* (% RA for *m/z* = 7660–7940) for $C_{559}H_{629}O_{27}$ $[M-OCH_3]^+$: 7779.9 (100), 7763.9 (55), 7748.0 (85), 7733.0 (50), 7716.9 (45); narrow range scan (label 1431.5x): *m/z* (% RA for *m/z* = 7660–7940) for $C_{559}H_{629}O_{27}$ $[M-OCH_3]^+$: 7780.2 (100), 7764.8 (40), 7748.8 (75), 7733.3 (35), 7716.6 (35); narrow range scan (label 1431.6xf): *m/z* (% RA for *m/z* = 7771–7788) for $[M-OCH_3]^+$: 7779.7 (100); calcd for $C_{559}H_{629}O_{27}$ at $[M-OCH_3]^+$: average mass = 7780.075; peak maximum mass = 7779.71; IR: $\tilde{\nu}$ = 1595 (Ar), 1082 cm^{-1} (C-O-C); ^1H NMR (500 MHz, C_6D_6, 293 K): δ = 6.90–8.20 (m, 224H), 2.80–3.20 (m, 84H), 0.70–1.50 ppm (m, 324H); ^1H NMR (500 MHz, [D_6]benzene, 293 K, ^1H–^1H DQF COSY, selected cross-peaks in the aromatic region): δ = 7.023 ppm (d, $J \approx 8$ Hz, 7.53).

Compound 5-$(OCH_3)_{42}$: Overall yield: 20.1 mg (6.8%) (sample labels: 1431.7x and 1431.8x); softening at 236°C, decomposition at 288–300°C; FABMS (ONPOE) wide range scan (label 1431.8x): *m/z* (% RA for *m/z* = 3200–13600): 3860 (100), 5828 (53), 6925 (17), 7779 (20), 9406 (15), 10120 (16), 11684 (39) $[M-OCH_3]^+$. narrow range scan (label 1431.8x): *m/z* (% RA for *m/z* = 3869–3880, baseline at about 20 in this range) for $C_{279}H_{313}O_{13}$ $[M-C_{561}H_{635}O_{29}]^+$: 3870.3 (42), 3871.3 (59), 3872.3 (81), 3873.3 (100), 3874.3 (97), 3875.3 (71), 3876.3 (70), 3877.3 (47), 3878.3 (38), 3879.3 (31); calcd for $C_{279}H_{313}O_{13}$ $[M-C_{561}H_{635}O_{29}]^+$: 3871.4 (19), 3872.4 (60), 3873.4 (95), 3874.4 (100), 3875.4 (79), 3876.4 (50), 3877.4 (27), 3878.4 (12), 3879.4 (5); narrow range scan (label 1431.8x) *m/z* (% RA for *m/z* = 11500–11850, baseline from 45 through 65 to 25 in this range) for $[M-OCH_3]^+$: 11683.3 (100), 11666.6 (80), 11651.8 (100), 11635.6 (80), 11620.5 (80); narrow range scan (label 1431.7x): *m/z* (% RA for *m/z* = 11500–11900, baseline from 45 through 65 to 25 in this range) for $[M-OCH_3]^+$: 11683.1 (100), 11666.9 (75), 11651.6 (100), 11635.0 (80), 11620.8 (85); calcd for $C_{839}H_{945}O_{41}$ $[M-OCH_3]^+$: average mass = 11685.765, peak maximum mass = 11685.45; IR: $\tilde{\nu}$ = 1595 (Ar), 1082 cm^{-1} (C-O-C); ^1H NMR (500 MHz, [D_6]benzene, 293 K): δ = 6.90–8.20 (m, 336H), 2.80–3.20 (m, 126H), 0.70–1.50 ppm (m, 486H).

Compound 12-$(OCH_3)_n$: Overall yield: 17.6 mg (6.5%) (label 1431.9x); softening at 236°C, m.p. 264–265°C, melted and turned brown; FABMS (ONPOE) wide range scan: *m/z* (% RA for *m/z* = 3200–13600): 3860 (100), 5500–6300 (~20), 7748 (44), 9200–10200 (~10), 11683 (29), 13200–13400 (~10); FABMS (3-NBA) wide range scan *m/z* (% RA for *m/z* = 3200–13600): 3860 (100), 4000–13600 (<5); IR: $\tilde{\nu}$ = 1595 (Ar), 1079 cm^{-1} (C-O-C); ^1H NMR (500 MHz, [D_6]benzene, 293 K): δ = 6.80–8.20 (m, 448H), 2.80–3.20 (m, 56H), 1.10–1.30 ppm (m, 648H).

Compound 6-$(OCH_3)_n$: Overall yield: 93.6 mg (31%) (label 1431.10TLC2x); brownish but not softening at 244°C, softening at 263°C, became more brownish and melting with decomposition at 290–292°C; IR: $\tilde{\nu}$ = 1595 (Ar), 1081 cm^{-1} (C-O-C); ^1H NMR (500 MHz, [D_6]benzene, 293 K): δ = 6.80–8.20 (m, 112*n*H), 2.80–3.20 (m, 42*n*H), 1.10–1.30 ppm (m, 162*n*H).

Acknowledgment

This research was supported by the National Science Foundation (Chemistry Division) grants to AR and the National Center for Neutron Research (beam time on NG3, grants No. 1781 and No. 2471). The mass spectrometry facility was supported in part by NIH Grant P20 RR15635 from the COBRE Program of the National Center for Research Resources, NCI Cancer Center Support Grant P30 CA36727, and the Nebraska Research Initiative. We thank Professor Richard Schoemaker for obtaining selected two-dimensional NMR data (TQF COSY, TOCSY, etc.). We thank Drs. Paul Butler and Sungmin Choi for technical assistance with the small angle neutron scattering experiments.

[1] A. Rajca, *Chem. Eur. J.* **2002**, *8*, 4834–4841.
[2] K. Itoh in *Molecular Magnetism, New Magnetic Materials* (Ed.: M. Kinoshita), Gordon and Breach, Kodansha, **2000**, pp. 1–337.
[3] P. M. Lahti, *Magnetic Properties of Organic Materials*, Marcel Dekker, New York, **1999**, pp. 1–713.
[4] A. Rajca, *Chem. Rev.* **1994**, *94*, 871–893.
[5] H. Iwamura, N. Koga, *Acc. Chem. Res.* **1993**, *26*, 346–351.
[6] K. Matsuda, N. Nakamura, K. Inoue, N. Koga, H. Iwamura, *Bull. Chem. Soc. Jpn.* **1996**, *69*, 1483–1494.
[7] T. Michinobu, J. Inui, H. Nishide, *Org. Lett.* **2003**, *5*, 2165–2168.
[8] H. Nishide, T. Ozawa, M. Miyasaka, E. Tsuchida, *J. Am. Chem. Soc.* **2001**, *123*, 5942–5946.
[9] R. J. Bushby, D. Gooding, *J. Chem. Soc. Perkin Trans. 2* **1998**, 1069–1075.
[10] M. M. Murray, P. Kaszynski, D. A. Kaisaki, W. Chang, D. A. Dougherty, *J. Am. Chem. Soc.* **1994**, *116*, 8152–8161.
[11] K. K. Anderson, D. A. Dougherty, *Adv. Mater.* **1998**, *10*, 688–692.
[12] N. Mataga, *Theor. Chim. Acta* **1968**, *10*, 372–376.
[13] A. Aharoni, *Introduction to the Theory of Ferromagnetism*, 2nd ed., Oxford University Press, Oxford **2000**, Chapter 4, pp. 76–79.
[14] a) For isotropic exchange coupling involving the Heisenberg Hamiltonian based models (generally applicable to organic polyradicals), the absence of ferromagnetism or antiferromagnetism in one or two-dimensions was rigorously proven: N. D. Mermin, H. Wagner, *Phys. Rev. Lett.* **1966**, *17*, 1133–1136; b) The Mermin-Wagner theorem was extended to additional models: P. Bruno, *Phys. Rev. Lett.* **2001**, *87*, 137203–1–4.
[15] For selected models, based upon anisotropic exchange coupling (e.g., Ising Hamiltonian), ferromagnetism in two-dimensional system is possible, see for example: R. P. Feynman, *Statistical Mechanics*, Benjamin/Cummings, Reading, MA, **1972**, Chapter 5, pp. 127–150.
[16] The magnetic dipole–dipole interactions may lead to ferromagnetism in two dimensions, though only at relatively low temperatures: Y. Yafet, J. Kwo, E. M. Gyorgy, *Phys. Rev. B* **1986**, *33*, 6519–6522.
[17] A. Rajca, J. Wongsriratanakul, S. Rajca, *Science* **2001**, *294*, 1503–1505.
[18] For a report on organic spin clusters addressing the possible source of magnetic anisotropy (shape anisotropy) in polymer **1** see: "Organic Spin Clusters: Dendritic-Macrocyclic Polyarylmethyl Polyradical with Very High-Spin of S = 10 and its Derivatives: Synthesis, Magnetic Studies, and Small Angle Neutron Scattering": S. Rajca, A. Rajca, J. Wongsriratanakul, P. Butler, S. Choi, *J. Am. Chem. Soc.* in press.
[19] For a report on organic spin clusters addressing the development of net ferri- or ferromagnetic correlations in polymer **1** see: "Organic Spin Clusters: Macrocyclic–Macrocyclic Polyarylmethyl Polyradicals with Very High Spin S = 5–13": A. Rajca, J. Wongsriratanakul, S. Rajca, *J. Am. Chem. Soc.* in press.
[20] A. Rajca, S. Rajca, J. Wongsriratanakul, *J. Am. Chem. Soc.* **1999**, *121*, 6308–6309.
[21] In the other limiting mode of annelation, the calix[4]arene macrocyles are connected through the diagonal benzene rings.
[22] A. Rajca, K. Lu, S. Rajca, *J. Am. Chem. Soc.* **1997**, *119*, 10335–10345.
[23] A. R. Forrester, J. M. Hay, R. H. Thomson, *Organic Chemistry of Stable Free Radicals*, Academic Press, London, **1968**, Chapter 2, pp. 55–110.
[24] A. Rajca in *Encyclopedia of Polymer Science and Technology*, 3rd ed. (Ed: J. I. Kroschwitz), Wiley, Online Posting Date: October, **2002**.
[25] All steps in the synthesis in Scheme 1 involve addition of *n*BuLi or *t*BuLi. Except for the first step, the μL volumes of solutions of butyllithium compounds are measured by counting drops from a calibrat-

ed syringe/needle set. Also, for the most recently completed reactions only, the butyllithium compounds were titrated directly prior to use. The last step in the synthesis of **11-$(OCH_3)_{27}H_2$** was carried out only once on the 4 μmol scale and involved addition of only 2 drops of the solution of *t*BuLi; this may contribute to the low yield of the product.

[26] Such "mono-demethylated" polyethers were observed by FAB-MS in other instances (e.g., ref. [19]).

[27] For analogous polyethers, which consists of two or three linearly connected calix[4]arene units, the $[M-OCH_3]^+$ and $[M-2OCH_3]^{2+}$ ions are the most prominent; other fragmentations are relatively insignificant (ref. [19]). Also, only the $[M-OCH_3]^+$ ion is prominent for **10-$(OCH_3)_{15}Br_2$**.

[28] GPC/MALS data for **5-$(OCH_3)_{42}$**, **12-$(OCH_3)_n$**, and polymer **6-$(OCH_3)_n$** were obtained under identical conditions.

[29] The chromatograms for mixture of **3-$(OCH_3)_{14}$** and **5-$(OCH_3)_{42}$** were resolved, as well.

[30] The values of R_g were obtained from the Guinier fits in the q range, for which $R_g q < 1.10$. The SANS experiments and the data handling are described in detail ref. [18]; a short summary may be found in the Supporting Information.

[31] General definitions of averages of S, including spin-weighed spin S_s, may be found in ref. [20] (note 21).

[32] This approximate mean-field approach is justified for such small values of $|\theta|$.

[33] Most likely, polymer **6** possesses net ferromagnetic couplings with a wide distribution of strengths.

[34] E. Beloritzky, P. H. Fries, *J. Chim. Phys. Phys.-Chim. Biol.* **1993**, *90*, 1077–1100.

[35] At higher magnetic field, $H = 0.5$ Tesla, the low temperature downward turn in the χT versus T plot is dominated by paramagnetic saturation; this is overestimated at low temperatures by the fit with the perfect $S = 7$ polyradical ($J/k > 0$), while $S \approx 6$ is found for the sample. At lower fields, the paramagnetic saturation nearly vanishes and antiferromagnetic interactions become detectable for the $J/k > 0$ case. At lower magnetic fields, the need for additional correction for diamagnetism may be caused by a low signal-to-noise ratio for the paramagnetic component, especially at higher temperatures.

[36] A. Rajca, J. Wongsriratanakul, S. Rajca, *J. Am. Chem. Soc.* **1997**, *119*, 11674–11686.

[37] These two-parameter percolation fits possess relatively large values of parameter dependence, approaching 0.99, making them less reliable than the two-parameter fits to a single Brillouin function.

Received: December 18, 2003

Published online: April 30, 2004

